

## REACTIONS OF WOOD DURING EARLY COALIFICATION, A CLUE TO THE STRUCTURE OF VITRINITE

Patrick G. Hatcher, Kurt A. Wenzel, Jean-Loup Faulon  
Fuel Science Program  
The Pennsylvania State University  
University Park, PA 16802

Keywords: vitrinite, coal structure, lignin, molecular modeling

### Introduction

Average structural models of coal have traditionally represented coal as a cross-linked macromolecular assemblage of interconnected fragments whose presence in the structure have been inferred from thermal or chemical degradative studies (1-4). To assemble such structures from a melange of fragments existing within some degradative product serves to homogenize a material which is inherently heterogeneous on a macromolecular scale. The structural representations fail to capture this heterogeneity, induced primarily by the existence of macerals representing macromolecularly distinct and possibly internally homogeneous physical entities derived from pre-existing vegetal matter in coal-forming swamps. More realistic structural models can be produced if the individual macerals are considered as discreet homogeneous domains within the heterogeneous mixture known as coal.

For the past several years we have been assembling structural models for individual macerals, focussing initially on vitrinite derived exclusively from xylem of gymnospermous wood (5-9). Studies of such xylem recovered from samples whose rank increases from peat to bituminous coal have provided a wealth of information concerning the molecular fragments and their reaction pathways as they undergo coalification to higher rank. We have been able to ascertain that lignin is the precursor of the vitrinite (5) and that, as such, we can build a structural model with lignin as a template (6, 8). Comparisons among the coalified xylem samples at various stages of coalification by elemental analysis, solid-state  $^{13}\text{C}$  NMR, and flash pyrolysis/gas chromatography/mass spectrometry (7,9) provides clues regarding the fate of the various oxygen-containing functional groups. Thus, working from a structural template and altering the template accordingly, a series of structural models representing vitrinite from gymnospermous xylem can be constructed at various rank levels.

Crucial aspects of this approach are 1) the accuracy of the structural model of lignin and 2) the accuracy with which we can define specific coalification reactions. In this paper, we focus on the effect of early coalification reactions on the three dimensional structure of lignin as a prelude to development of a comprehensive model for vitrinite at later stages of coalification.

### Coalification Reactions of Lignin

There is mounting evidence that lignin is not a random heteropolymer but an ordered structure. Faulon and Hatcher (10) have recently suggested that lignin assumes an helical conformation of  $\beta$ -O-4-linked glyceryl methoxyphenolic ethers. Although we have used a random structure as a template in previous studies (6, 8), we have now adopted this helical model, shown in Figure 1, as the template.

As coalification of lignin proceeds, some key reactions will modify the chemistry and three dimensional helical structure. Random, large-scale structural reorientations of lignin will likely destroy delicate physical attributes such as bordered pits and cellular walls. The fact that these

physical characteristics of wood persist to the rank of subbituminous coal suggests that the early coalification reactions are likely to be those which cause minimum distortion of the three dimensional structure.

Perhaps the most readily apparent reaction observed in numerous studies (7, 11-13) is the demethylation of lignin. We expect that this reaction has no significant effect on the helical conformation other than to perhaps facilitate hydrogen bonding interactions between helices, because the methyl group is replaced by a hydrogen. The helix is well preserved by this reaction with virtually no change in the cross-sectional size of the helix.

Another reaction which might be expected to induce minimal distortion of the helical structure is dehydroxylation of the hydroxyl groups on side-chain carbons. It is clear from NMR spectra of coalified wood samples at the rank of subbituminous coal that virtually no significant resonances are observed for hydroxylated aliphatic structures, suggesting complete dehydroxylation. Because the aromaticity does not change during this early coalification, we believe that hydroxyl groups have been reduced to alkyl structures. The  $sp^3$  hybridization does not change as a result of this process and, thus, the helical order is not disrupted.

The most significant coalification reaction noted in previous studies (6,8) which has an impact on the helical conformation of lignin is the hydrolysis of the  $\beta$ -O-4 aryl ethers. Rupture of this bond, the primary bond maintaining the structural integrity of the helix, would essentially dismantle the lignin and reduce it to small molecules. If this hydrolysis is the sole reaction, then the lignin would likely be solubilized and removed from the coal. The NMR evidence shows that hydrolysis of the  $\beta$ -O-4 aryl ethers does occur, but a concerted alkylation of an adjacent aromatic ring by the side-chain carbocation formed as the result of hydrolysis maintains the structural integrity of the lignin. The evidence forwarded for such a concerted reaction is manifold. First, evidence for hydrolysis of the  $\beta$ -O-4 aryl ether, though weak, is a decrease in the peak intensity of aryl-O ether carbons in NMR spectra (7). Evidence for increased substitution is provided by dipolar dephasing data which shows a decrease in the average number of protons per ring during the transformation of lignin to brown coal (6). Artificial coalification by Botto (14) of a lignin labeled at the  $\beta$  site shows alkylation to be a significant part of early coalification. The proposed scheme involves cleavage of the  $\beta$ -O-4 aryl ether followed by alkylation of an adjacent ring by the resulting carbocation (8).

Molecular modeling simulations in three dimensional space shows that such a reaction maintains the helical structure of lignin as well as its macromolecular nature (Figure 2). The helix formed by linkages between the  $\beta$  site and the adjacent aromatic ring is of a larger radius and pitch. We would expect that the increased radius of the helix might be expressed at the macroscopic level. Thus, as lignin helices which collectively comprise the cell walls of the peatified wood samples are transformed to helices with larger radii, the cell walls would be expected to show a corresponding size change. Because the axes of the helices are thought to align parallel to the cell walls, any increase in radius will induce cell-wall thickening. Thickening of the cell wall is commonly observed during coalification (15). Photomicrographs depicting the cross-sectional views of peatified wood, composed of essentially pure lignin, and coal wood of subbituminous rank, composed of coalified lignin having undergone cleavage of  $\beta$ -O-4 ethers, alkylation of aromatic rings, and side-chain dehydroxylations, are shown in Figure 3. It is clear that the cell walls are thicker in the brown coal wood, compared with peatified wood. Thus, the model of low-rank coal as a modified helical lignin structure can explain both the observed chemistry and physical morphology.

## Conclusions

The modeling of lignin as a helical structure has important implications regarding the structure of vitrinite in coal. If one uses this lignin as a template for coalification, then chemical

changes induced by coalification reactions are likely to affect the helical order. The changes observed in previous investigations do modify the helical structure but fail to entirely disrupt it. These changes are primarily demethylation, side-chain dehydroxylation, and cleavage of the  $\beta$ -O-4 ethers in concert with alkylation of aromatic rings. The three-dimensional changes in the helical order brought about by these reactions are consistent with observed morphological changes in the coalified wood.

#### Literature Cited

1. Given, P. H., *Fuel*, **39**, 147, 1960.
2. Wisler, W. H., *Proc. of the Electric Power Research Institute Conf. on Coal Catalysis*, 1973.
3. Solomon, P.R., in *New Approaches in Coal Chemistry*, Am. Chem. Soc. Symp. Series No. **169**, 61, 1981.
4. Shinn, J. H., *Fuel*, **63**, 1187, 1981.
5. Hatcher, P.G., Breger, I.A., Earl, W.L., *Organic Geochemistry*, **3**, 49, 1981.
6. Hatcher, P.G., *Energy and Fuels*, **2**, 48, 1988.
7. Hatcher, P.G., Lerch, H.E., III, and Verheyen, T.V., *Int. J. Coal Geol.*, **13**, 65, 1989.
8. Hatcher, P. G., *Organic Geochemistry*, **16**, 959, 1990.
9. Hatcher, P.G., Lerch, H.E., III, Kotra, R.K., and Verheyen, T.V., *Fuel*, **67**, 1069, 1988.
10. Faulon, J. L. and Hatcher, P. G., *Naturwissenschaften*, (in press).
11. Stout, S. A., Boon, J. J. and Spackman, W., *Geochim. Cosmochim. Acta*, **52**, 405, 1988.
12. Hedges, J.J., Cowie, G.L., Ertel, J.R., Barbour, R.J., and Hatcher, P.G., *Geochimica et Cosmochimica Acta*, **49**, 701, 1985.
13. Ohta, K. and Venkatesan, M. I., *Energy & Fuels*, **6**, 271, 1992.
14. Botto, R. E. *Energy & Fuels*, **1**, 228, 1987.
15. Stach, E., Taylor, G. H., Mackowski, M-Th., Chandra, D., Teichmüller, M. and Teichmüller, R. *Stach's Textbook of Coal Petrology*, Gebrüder Bornträger, Berlin, 428pp.

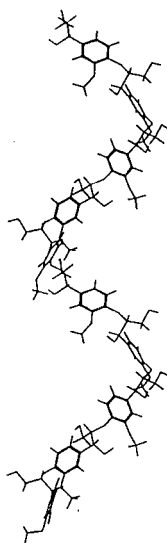


Figure 1. Three dimensional helical conformation for the structure of lignin. This structure has been obtained after energy minimization. The structure is composed of the main monomer (guaiacyl) and linkage type ( $\beta$ -O-4) occurring in lignin.

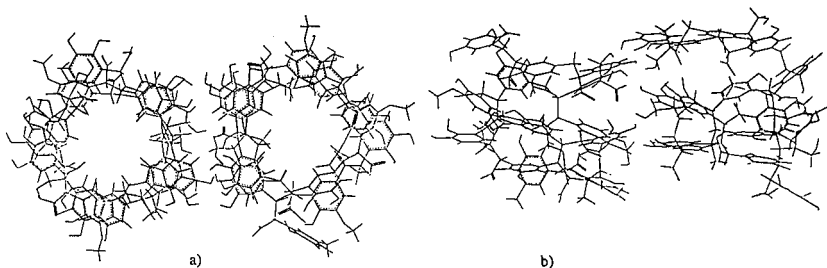
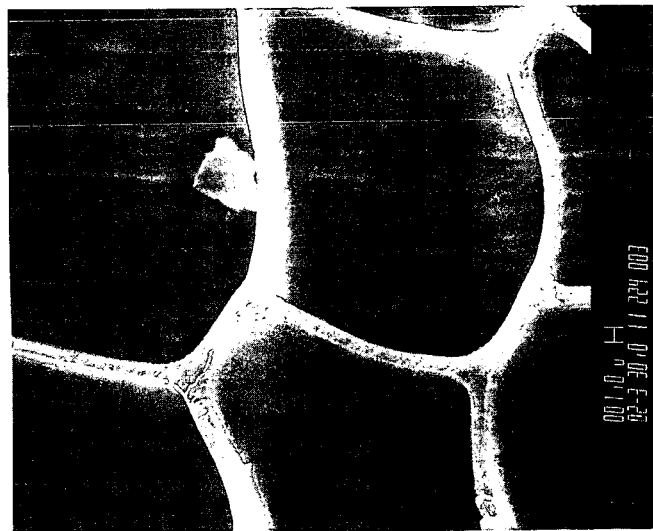


Figure 2. Three dimensional conformation for a lignite rank coalified wood. This lignite structure was obtained by using two helical lignin structures as a template. The initial lignin structures were modified as describe in the text, then, the resulting structure was submitted to molecular mechanics and dynamics simulations to obtained the lowest energy conformation. a) Three-dimensional representation of the structure in plan view. b) Three-dimensional representation of the structure viewed from the side.



a)



b)

Figure 3. SEM photographs of a) degraded wood, and b) subbituminous coalified wood. The two photographs have been taken with the same resolution (the scale indicated at the bottom of the photographs is 1  $\mu\text{m}$ ).

## STATISTICAL EVALUATION OF PHYSICAL PROPERTIES FOR COAL MACROMOLECULES BASED ON COMPUTER-GENERATED STRUCTURES

Jean-Loup Faulon<sup>1</sup>, Gary A. Carlson<sup>2</sup>, Jonathan P. Mathews<sup>1</sup>, and Patrick G. Hatcher<sup>1</sup>.

<sup>1</sup>Fuel Science Program, The Pennsylvania State University, University Park, PA 16802.

<sup>2</sup>Fuel Science Dept., Sandia National Laboratories, Albuquerque, NM 87110.

Keywords : CAMD, Coal structure, Fractal dimension.

### INTRODUCTION

Computer-Aided Molecular Design (CAMD) has recently been introduced in the area of coal science (1-6). Carlson and co-workers (1) used CAMD to model in three dimensions previously published coal structures. The structures were submitted to molecular mechanics and dynamics. The potential energy, the true density, and the microporosity were evaluated for each model (2). Nomura and co-workers have also used CAMD to study their own coal model (3). Using molecular dynamics with periodic boundary conditions, Murata (4) correlated potential energy and true density. An important point needs to be mentioned regarding the utilization of CAMD for the study of coal; prior to use of CAMD software, the connectivity (i.e. the structural formula) of the studied molecule has to be known. This information is unfortunately lacking for coal.

Many studies (7) have been conducted in the past 25 years to resolve by computer the general problem of retrieving a structure from analytical data. The generic name for these studies is Computer-Aided Structure Elucidation (CASE). We recently developed a new CASE technique (the SIGNATURE program ref. 8) for the modeling of complex macromolecules. The technique is able to construct large molecular models from analytical structural data and has already been applied to devise models for vitrinite maceral from HvC bituminous coal (5,6). Aside from constructing models in three-dimensional space, the SIGNATURE program is also able to compute the number of models possible (7). Knowledge of this number is crucial to our being able to decide how many models are necessary to represent coal. Even if this number is too large to allow all the models to be built, sampling theory makes it possible to select a subset of models (a sample) which is statistically representative of the whole population (9). Among the various techniques of sample design, the Simple Random Sampling Without Replacement (SRSWOR ref. 9) is the most convenient to apply here. The SIGNATURE program can directly build the required sample because the program permits the construction of non-identical random models.

### METHOD

The experimental material chosen for this study was a piece of coalified wood, specifically a fossil stem which was recovered from a lacustrine shale from the Midland Formation (Triassic) near Culpeper, Virginia. In a previous report (10), we assumed that this coalified wood is representative of vitrinite from HvC bituminous coal. The analytical data supplied to the SIGNATURE program (published earlier, ref. 10) are summarized in Table I. The SIGNATURE program was run and all the solutions containing 333 carbon atoms were searched. This number of carbons was chosen considering the computational time and the fact that all the fragments listed in Table I must be present in the models. The SIGNATURE program found only five different molecular formulas (Table II) having a deviation between model and analytical data less than 1%.

As presented in Table II, the population of possible coal models is subdivided into five different C<sub>333</sub> structures. To build a sample which is a good representation of the entire population, the sample size of each C<sub>333</sub> structure has to be proportional to the corresponding population of all of its possible isomers. Considering the population size of each C<sub>333</sub> structures (Table II) and the computational time required to build the structures and evaluate the different

characteristics, we chose to build a sample of  $n_1 = 15$  structures comprising the following: 2 structures of  $C_{333}H_{302}O_{16}$ , 10 structures of  $C_{333}H_{304}O_{16}$ , 1 structure of  $C_{333}H_{306}O_{16}$ , 1 structure of  $C_{333}H_{308}O_{16}$ , and 1 structure of  $C_{333}H_{310}O_{16}$ . For each of the 15 models, minimum energy conformations were calculated using a procedure described in a previous report (5). Then, physical characteristics were evaluated using a program initially devised to compute the physical true density (2,5), and updated to determine the micropore volume (6). In the present paper, the program was extended in order to compute the surface area. Briefly, the surface area is computed by immersing the molecular model in a grid composed of cubic cells of length  $r$  (generally  $r = 1 \text{ \AA}$ ). We define two types of surface area - the total surface area, and the pore surface area. The total surface area represents the actual surface of the structure. This surface is computed by summing all the areas of cell faces tangent to the Van der Waals sphere of an atom. The pore surface area is the surface of the micropore volume. The pore surface is computed by summing of the areas of cell faces which belong to a micropore cell (i.e. a cell located inside a micropore) and are tangent to the Van der Waals sphere of an atom.

The results for the physical characteristics are presented in Fig. 1. Means and variances were calculated using the SWRSOR procedure developed by Cochran (9).

## DISCUSSION

All 15 of the constructed  $C_{333}$  models agree well with the quantitative analytical data with an average deviation of less than one percent. The number of cross-links varies between 2.5 and 5 for each  $C_{333}$  structure, and the molecular weight per cross-link averages 1205 amu with a standard deviation of 254 amu. This value agrees well with swelling experiments for acetylated and pyridine extracted bituminous coal, where the molecular weight per covalent cross-link ranges between 900 and 1500 amu (11). Furthermore, the average number of aromatic fragments between cross-links (7.9) is in the range of values obtained from swelling experiments (4-8 aromatic fragments between cross-links ref. 11,12).

Fig. 1 shows that the potential energy increases slightly with the number of cross-links (1.85 kcal/atom for the model having 2.5 cross-links and 2.14 - 2.16 kcal/atom for the two models having 5 cross-links). However, overall, the energy values are clustered, and as a direct consequence, the variance is small (Fig. 1). Another interesting point was observed when the structures were depicted on the computer monitor. Independent of the cross-link density, the global conformations appeared very similar. This suggests that even when the structures are not highly covalently cross-linked, they are held together by van der Waals interactions. A related observation is that no major changes in helium density and porosity were observed for the models investigated containing different cross-link densities (Fig. 1).

The computed helium density averages 1.26 g/cc for all 15  $C_{333}$  structures constructed with the population deviation being less than 2 percent. This result is in good agreement with experimental results found for vitrinite at a rank of bituminous coal (1.25 - 1.30 g/cc, ref. 13). The computed micropore volume averages 0.030 cc/g with a population deviation of 13 percent. The micropore volume is slightly lower than experimental values found for coals of HvC bituminous rank (0.039 - 0.070 cc/g, ref. 14). The low microporosity may be due to the size of our models; they are very small compared to the particle sizes used in porosimetry experiments.

The calculated total surface area for all of the 15 models averages  $3693 \pm 29 \text{ m}^2/\text{g}$ . This is at least 10 times larger than the values measured by  $\text{CO}_2$  absorption, and about 100 times larger than the BET surface area obtained with  $\text{N}_2$  for the same rank of coal (15). However, the calculated total surface area cannot be correlated with experimental results because the sizes of our models are small, and the external surfaces (surfaces of the boundaries of the structures) are much larger than the internal surfaces (surfaces of the micropores). This contrasts with experimental results, where the external surface area is negligible compared to the internal surface area (15).

Since the micropore surface area is dominant experimentally, we should expect our pore surface calculation to be in better agreement with experimental results. We find the micropore surface area calculated for our models is relatively close to the  $\text{CO}_2$  surface area measured for HvC

bituminous coal (120-250 m<sup>2</sup>/g, ref. 15). Our mean value (292 m<sup>2</sup>/g) is slightly larger than experimental values, probably due to our calculation method. Our method for surface calculations uses a cell grid size of 1 Å length. The same calculations made with a doubled grid size (2 Å) for the first C<sub>333</sub> structure of the sample (C<sub>333</sub>H<sub>302</sub>O<sub>16</sub>) gives a micropore surface area of 190 m<sup>2</sup>/g. It is known that the surface area of coal behaves like a fractal surface (16-19); therefore, an increase in the cell size leads to a decrease in the surface area. Fig. 2 correlates on a log-log scale different sizes of the cell grid and the number of cells which belong to the pore surface for the structure C<sub>333</sub>H<sub>302</sub>O<sub>16</sub>. According to Pfeifer and Avnir (20), the negative slope of the line is the fractal dimension (D = 2.68 in the example of Fig. 2). The fractal dimension of the total surface area was also calculated for each of the C<sub>333</sub> models comprising the sample using a cell grid size varying between 1 Å and 8 Å (Fig. 3). Using the SRSWOR technique, the mean value found was D = 2.71 and the population deviation found was only 0.05.

In summary, we have been able to develop a technique that uses the power of the computer to create a number of molecular models for coal using actual quantitative and qualitative experimental data, and to show that the models, from a statistical viewpoint, are a good representation of the coal structure. Previous attempts to elucidate the molecular structure of coal, including previous computer models, necessarily included investigator bias and could not be proven to be representative or average coal structures. In the present study, we can conclude that for the physical properties investigated, a sample of 15 structures is sufficient to represent statistically the whole population of vitrinite from HvC bituminous.

## REFERENCES

1. Carlson, G. A.; Granoff B. In *Coal Science II*: Schobert H. H., Bartle, K. D. Eds., ACS Symp. Ser. 461, Washington, DC, 1991, pp. 159.
2. Carlson, G. A. *Energy & Fuels* **1992**, *6*, 771.
3. Nomura, M.; Matsubayashi, K.; Ida, T.; Murata, S. *Fuel Process. Technol.* **1992**, *31*, 169.
4. Murata, S. 1992, personal communication.
5. Faulon, J. L.; Hatcher, P. G.; Carlson, G. A.; Wenzel, K. D. *Fuel Process. Technol.* in press.
6. Faulon, J. L.; Carlson, G. A.; Hatcher, P. G. *Energy & Fuels* in press.
7. Smith, D. H. *Computer-Assisted Structure Elucidation*: ACS Symp. Ser. 54, Washington, DC, 1977.
8. Faulon, J. L. *Prediction Elucidation and molecular modeling*. PhD Thesis, Ecole des Mines, Paris, 1991; Faulon, J. L. *J. Chem. Inf. Comput. Sci.* **1992**, *32*, 338.
9. Cochran, W. G. *Sampling Techniques* (3rd Ed.); John Wiley & Sons: New York, 1977.
10. Hatcher, P. G.; Faulon, J. L.; Wenzel, K. A.; Cody, G. D. *Energy Fuels* **1992**, *6*, 813.
11. Larsen, J. W.; Green, T. K.; Kovac, J. J. *Org. Chem.* **1985**, *50*, 4729.
12. Hall, P. J., Marsh, H.; Thomas, K. M. *Fuel* **1988**, *67*, 863.
13. Crelling, J. C. *Proc 1987 Int. Conf. Coal Sci.* **1987**, 119.
14. Gan, H.; Nandi, S. P.; Walker, P. L., Jr. *Fuel* **1972**, *51*, 272.
15. Mahajan, O. P. *Coal Porosity In Coal Structures*; Meyers, R. A., Ed.; Academic Press: New York, 1982; pp 51-86.
16. Bale, H. D.; Schmidt, P. W. *Phys. Rev. Lett.* **1984**, *53*, 596.
17. Friesen, W. I.; Mikula, R. J. *J. Colloid Interface Sci.* **1987**, *120*, 268.
18. Reich, M. H.; Russo, S. P.; Snook, I. K.; Wagenfeld, H. K. *J. Colloid Interface Sci.* **1990**, *135*, 353.
19. Reich, M. H.; Snook, I. K.; Wagenfeld, H. K. *Fuel* **1992**, *71*, 669.
20. Pfeifer, P.; Avnir, D. *J. Chem. Phys.* **1983**, *79*, 3558.

ACKNOWLEDGEMENTS : Funding was provided by the U.S. Department of Energy at Sandia National Laboratories under contract DE-AC04-76DP00789.

**Table I.** Analytical data for HvC Bituminous coalified wood (Midland Stem, ref. 10).

Parameter	Analytical Data	Model (C <sub>333</sub> H <sub>302</sub> O <sub>16</sub> )	Deviation Analytical data - Model
<b>Elemental analysis and carbon-13 NMR data (normalized for 100 carbon atoms)</b>			
C	100.0	100.0	-
H	92.0	91.8	0.2
O	5.0	4.6	0.4
f <sub>a</sub> (aromatic carbon)	62.5	63.0	-0.5
f <sub>a</sub> <sup>H</sup> (protonated aromatic carbon)	28.0	27.6	0.4
f <sub>a</sub> <sup>P</sup> (phenolic or phenolic ether)	7.5	7.5	0.0
f <sub>al</sub> (aliphatic carbon)	37.5	37.4	0.1
f <sub>al</sub> <sup>H</sup> (aliphatic CH or C <sup>H</sup> <sub>2</sub> )	26.0	26.2	-0.2
f <sub>al</sub> <sup>*</sup> (aliphatic CH <sub>3</sub> )	11.5	11.2	0.3
Average deviation			± 0.26
<b>Flash Pyrolysis/gc/ms data (weight % normalized to total aromatic fragments)</b>			
benzene	3.3	2.0 (1)	1.3
toluene	4.8	4.8 (2)	0.0
C-2 benzenes	5.2	8.3 (3)	-3.1
C-3 benzenes	3.9	6.3 (2)	-2.4
phenol	3.6	2.5 (1)	1.1
<i>o</i> -cresol	5.7	2.8 (1)	2.9
<i>m</i> + <i>p</i> -cresol	13.0	8.5 (3)	4.5
2,4 dimethylphenol	12.0	9.6 (3)	2.4
other C-2 phenols	10.3	6.4 (2)	3.9
C-3 phenols	10.9	14.2 (4)	-3.3
C-4 phenols	4.8	3.9 (1)	0.9
alkylnaphthalenes	17.0	24.4 (6)	-7.4
alkyldibenzofurans	5.2	6.2 (1)	-1.0
methyl	-	(7)	
ethyl	-	(9)	
propyl	-	(3)	
C4-C22	-	(0)	

Values in parentheses are the quantities of each fragment corresponding to a molecule containing 333 carbon atoms.

**Table II.** Deviation analytical data - model and population information for each of the C<sub>333</sub> molecular formula<sup>a</sup>

Molecular Formula	Average deviation <sup>b</sup>	Number of possible models
C <sub>333</sub> H <sub>302</sub> O <sub>16</sub>	0.26	52,272
C <sub>333</sub> H <sub>304</sub> O <sub>16</sub>	0.29	231,000
C <sub>333</sub> H <sub>306</sub> O <sub>16</sub>	0.39	24,750
C <sub>333</sub> H <sub>308</sub> O <sub>16</sub>	0.49	9,856
C <sub>333</sub> H <sub>310</sub> O <sub>16</sub>	0.71	1,440

<sup>a</sup> The numbers of possible models have been estimated using the isomer generator provided by the SIGNATURE program (8). <sup>b</sup> The deviation is the average deviation between model and quantitative analytical data as calculated in Table I.

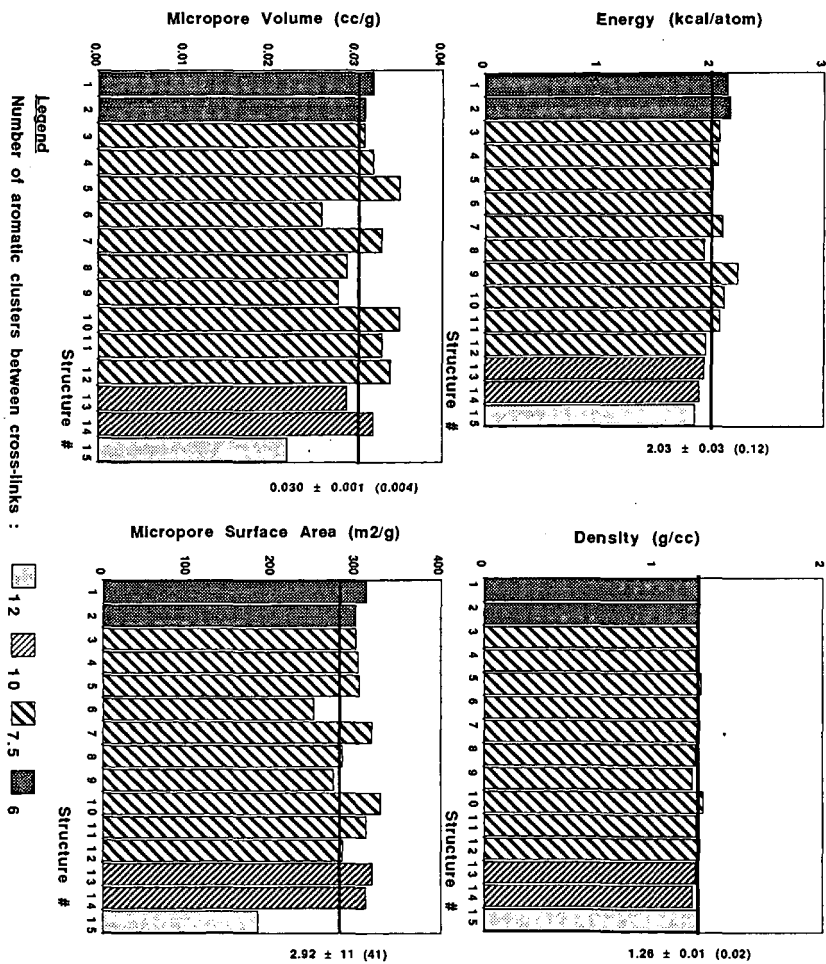


Fig.1. Correlation between physical characteristics and cross-link densities for each of the 15 individual models comprising the sample. For each graph, the horizontal line represents the population mean. The population deviations are indicated in parentheses.

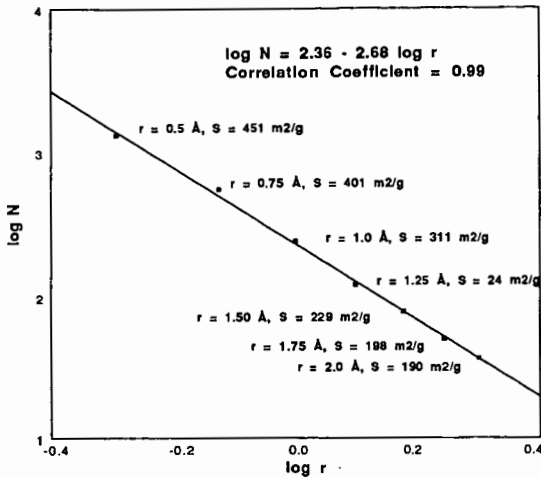


Fig. 2. Effect of the cell grid size on the micropore surface area for the first model of the sample ( $C_{333}H_{302}O_{14}$ ).  $N$  is the number of cell faces which belong to the surface of micropore volume,  $r$  is the size of the cells used in the surface area calculations (cf METHOD). The fractal dimension ( $D$ ) is defined by the following equation:  $N \propto r^{-D}$  or  $\log N \propto -D \log r$

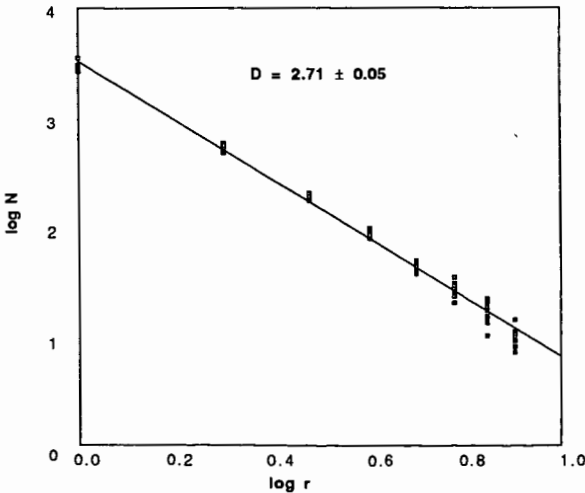


Fig. 3. Fractal dimension of the total surface area for the 15 models comprising the sample.  $N$  is the number of cell faces which belong to the surface of the models,  $r$  is the size of the cells used in the surface area calculations (cf METHOD).

## **CHANGES IN MOLECULAR BIOMARKER AND BULK CARBON SKELETAL PARAMETERS OF VITRINITE CONCENTRATES AS A FUNCTION OF RANK.**

Gordon D. Love\*, Colin E. Snape\* and Andrew D. Carr<sup>‡</sup>

\* University of Strathclyde, Department of Pure & Applied Chemistry,  
Glasgow G1 1XL, UK.

<sup>‡</sup> British Gas plc, London Research Station, Michael Road, London SW6 2AD, UK.

**Keywords:** Biomarkers, Vitrinite Reflectance, Solid State <sup>13</sup>C NMR.

### **ABSTRACT**

A sequential extraction scheme to differentiate between molecular alkanes and those covalently-bound to the macromolecular structure has been applied to a suite of vitrinite concentrates handpicked from six UK bituminous coals covering the rank range (%R<sub>o</sub> = 0.46-1.32 at 546 nm). The aim was to ascertain whether the biomarker indices (i) were consistent with the measured vitrinite reflectance values, especially for the lower rank members of the suite where reflectance measurements are unreliable and (ii) differ markedly for the easily extractable, clathrated and covalently-bound phases. The quantitatively reliable single pulse excitation (SPE) solid state <sup>13</sup>C NMR technique has also been used to elucidate the changes in the bulk vitrinite structure across the relatively narrow rank range investigated. Although both hopane and methylphenanthrene parameters for easily extractable species are sensitive to small variations in vitrinite reflectance, significant variations have been found between the biomarker parameters for easily extractable, clathrated and covalently-bound material. In general, restricted motions in the macromolecular structure make the latter less mature, as reflected by hopane and phenanthrene parameters, than the easily extractable and clathrated molecular species. Solid state <sup>13</sup>C NMR revealed that the variations in carbon aromaticity and the degree of condensation of the aromatic structure occurring in the %R<sub>o</sub> range of ca 0.45-0.80 are relatively small.

### **INTRODUCTION**

Biological markers are compounds detected in the geosphere derived from living organisms whose basic carbon skeleton has survived the processes of diagenesis and thermal maturation. The most commonly studied biomarkers are the cyclic alkanes; the hopanes and the steranes, which are derived from hopanoid and steroid natural products respectively, and are ubiquitous components of crude oils, kerogens and coals. As well as providing information about the original biological input to sediments, the distribution of certain hopane and sterane stereoisomers have been widely used to indicate the thermal stress experienced by fossil organic matter (see, for example, Fu Jiamo et al (1), Chaffee et al (2) and Mackenzie (3) and references therein for comprehensive reviews). The biologically synthesised conformations of their precursors are not the most thermally stable and configurational isomerisation is observed at certain chiral centres as maturation proceeds. Although these biomarkers are generally only present in small quantities (<< 1% w/w) in solvent extracts and pyrolysates, they are readily detectable using single ion monitoring in gas chromatography-mass spectrometry (GC-MS) without the need for extensive pre-separation (1-3).

To summarise, the hopanes are pentacyclic triterpanes which are believed to be derived from a C<sub>35</sub> triterpene alcohol, bacteriohopane-tetrol, a constituent of the membranes of bacteria other than Archaeobacteria. A series of C<sub>27</sub>-C<sub>35</sub> hopanes is the most commonly observed distribution in ancient sediments but usually the C<sub>28</sub> member is missing (1-3). The biological 17β(H), 21β(H) configuration inherited by the alkanes of immature sediments is lost rapidly with increasing maturity forming a mixture of 17α(H), 21β(H) and 17β(H), 21α(H) stereochemistries. Eventually the 17β(H), 21α(H)-hopanes also convert to the 17α(H), 21β(H) form. The sterol precursors of the tetracyclic steranes are widely distributed in nature and the most commonly encountered

steranes are those of carbon number C<sub>27</sub>, C<sub>28</sub> and C<sub>29</sub> although variable amounts of C<sub>21</sub> and C<sub>22</sub> isomers with shorter alkyl sidechains are also often present. At the later stages of diagenesis, the main steroidal components are usually alkanes and Ring C monoaromatics. Further maturation leads to configurational isomerisation, aromatisation of C-ring monoaromatic steroids to ABC-ring triaromatics (substituted phenanthrenes, see below) and enrichment of the lower molecular weight (MW) components (C<sub>20</sub>-C<sub>22</sub>) relative to the higher MW counterparts (C<sub>26</sub>-C<sub>29</sub>).

The Methylphenanthrene Index (MPI) proposed by Radke et al.<sup>(4)</sup> is a widely used maturity parameter based on their distribution in solvent extracts. Steroids and triterpenoids are probable biological precursors with their degradation and aromatisation yielding only 1- and 2- MP isomers. The 3- and 9-MPs arise as a result of methylation of phenanthrene and rearrangement of mono-methyl phenanthrenes. Radke et al.<sup>(4-6)</sup> observed that the relative amounts of 2- and 3- MP increase compared to the 1- and 9- isomers with increasing burial and depth. An empirical correlation (MPI 1, see Table 3) was then devised based on the distribution of these compounds relative to the amount of phenanthrene which could predict vitrinite reflectance values (% R<sub>c</sub>) for the samples studied.

The above molecular indices are usually calculated by observing the distribution of the appropriate biomarkers obtained by low temperature extraction using chloroform, dichloromethane (DCM) or methanol (or their mixtures). Since this type of treatment removes only a small proportion of the total organic matter (usually <5% w/w), it does not follow that the distributions of biomarkers are necessarily representative of those covalently bound to the macromolecular structure. Indeed, previous studies using low severity catalytic hydrogenation have established that in lignites<sup>(7)</sup>, kerogens<sup>(8)</sup> and a high volatile bituminous coal<sup>(7)</sup>, hopanes and steranes can be incorporated into the polymeric backbone via functional groups present in the original biolipids whilst retaining their less thermodynamically stable biological configurations. Thus, it appears that compounds covalently bound to the macromolecular network may be less sensitive to thermal alteration. Furthermore, it is known that coals contain a significant amount of physically trapped, low MW moieties which are inaccessible to treatment with the solvents mentioned above<sup>(9-11)</sup>. However, these components can partly be removed when more powerful solvents like pyridine or binary solvent mixtures<sup>(12)</sup> destroy the stronger non-covalent interactions within the macromolecular matrix<sup>(13)</sup>. This phase may contain significant amounts of biomarker species which may have a different distribution to those detected in the usual solvent or hydrogenation extracts. This prompted the authors to develop a sequential degradation scheme to help differentiate between easily extractable and clathrated species and moieties which were covalently-bound through weak heteroatomic bonds or more stronger C-C bonds. After an initial DCM soxhlet extraction, refluxing in pyridine allows the removal of more occluded material. Mild batchwise hydrogenation using a dispersed sulphided molybdenum (Mo) catalyst is then performed to cleave weak ester, ether and sulphide linkages. A final hydrolysis step in a fixed-bed reactor using a hydrogen sweep gas can render a significant proportion of the organic residue soluble in DCM (typically over 50% daf basis).

The sequential scheme has been applied here to a suite of vitrinite concentrates handpicked from six UK bituminous coals covering the rank range (%R<sub>o</sub> = 0.46-1.32 at 546 nm) which corresponds to a maturity range from just before to just after the so called "oil-generating window" for Type III materials. The aim of this investigation has been to ascertain whether the biomarker indices (i) were consistent with the measured %R<sub>o</sub> values, especially for the lower rank members of the suite where reflectance measurements are unreliable and (ii) differ markedly for the easily extractable, clathrated and covalently-bound phases.

As indicated above, the chemically-bound moieties appear to be more resistant to geothermal stress than molecules in the bitumen phase suggesting that a detailed chemical analysis of solvent extracts may not give a valid representation of the total organic structure. Thus, solid state <sup>13</sup>C NMR has been used to elucidate the changes in the bulk vitrinite structure across the relatively narrow rank range using the quantitatively reliable single pulse excitation (SPE) measurements. Previous investigators have correlated vitrinite reflectance with aromaticities derived from cross polarisation

(CP) (14-17), but it is now generally accepted that CP can strongly discriminate against aromatic carbons in fossil fuels (17-19).

## EXPERIMENTAL

The proximate and ultimate analyses, maceral compositions and measured average vitrinite reflectance values for the samples investigated are summarised in Table 1.

**Solvent Extractions** Each sample was ground to <150 $\mu$ m, dried in a vacuum oven at 50°C for 24 hours and then Soxhlet extracted with dichloromethane (DCM) for 72 hours. The solid residue (2-5g) was then refluxed rapidly with 200 cm<sup>3</sup> boiling pyridine (3 x 45 mins). The soaking time in pyridine was relatively short to prevent the structure rearranging to a more tightly bound conformation due to the formation of more non-covalent interactions (21). After each reflux step, the solids were washed in a DCM/ methanol solvent mixture (3:1 v/v) and then dried *in vacuo* to remove as much entrained pyridine as possible.

**Catalytic Hydrogenation and Fixed-Bed Hydroxyprolysis** Catalyst impregnation of solvent-extracted vitrinites was performed as described previously (22) with aqueous / methanol solutions of the precursor, ammonium dioxodithiomolybdate [(NH<sub>4</sub>)<sub>2</sub>MoO<sub>2</sub>S<sub>2</sub>], to give a nominal Mo loading of 1% daf coal. Batchwise hydrogenation runs were conducted at 300°C and 70 bar hydrogen pressure (ambient) in 7 cm<sup>3</sup> stainless steel microreactors constructed from Autoclave Engineers fittings. The microreactors were immersed in a fluidised sandbath for 60 mins. After cooling the reaction products were recovered in DCM, refluxed and then filtered to remove the DCM-insoluble residues and to determine overall conversions. The procedure for temperature-programmed hydroxyprolysis has been described in detail elsewhere (22)

**Product Work-up and Analysis** The DCM-soluble products from each stage of the extraction procedure were dried to constant weight in a stream of dry nitrogen. These were then separated by open-column silica gel adsorption chromatography into alkanes, aromatics and polars by eluting successively with n-hexane, n-hexane-toluene (1:1 v/v) and DCM/methanol (2:1 v/v). The yields were determined by transferring relatively concentrated solutions of the fractions into pre-weighed screw-cap vials and evaporating the residual solvent under a stream of nitrogen. GC-MS analysis was performed on the alkane and aromatic fractions using a Finnigan MAT TSO70 coupled to a Varian 3400 GC. For the alkanes, the single ions monitored were m/z 191 (for triterpanes) and 217 (for steranes). The sterane standards, 5 $\beta$ (H)-cholane and 20-methyl-5 $\alpha$ (H)-pregnane (Chiron Labs, Trondheim), was added to selected samples before injection.

**Solid State <sup>13</sup>C NMR Spectroscopy** All the <sup>13</sup>C NMR measurements were carried out at 25 MHz on a Bruker MSL100 spectrometer with MAS at 4.5-5.0 kHz to give spectra in which the sideband intensities are only ca 3% of the central aromatic bands. The vitrinites were vacuum dried and then ca 250 mg of sample was packed into the zirconia rotors. The <sup>1</sup>H decoupling and spin-lock field was ca 60 kHz and, for SPE, the 90° <sup>13</sup>C pulse width was 4.5  $\mu$ s. <sup>13</sup>C thermal relaxation times (T<sub>1s</sub>) of the vitrinites were determined using an appropriate CP pulse sequence with a contact time of 5 ms in most cases.

A relaxation delay of 20 s was used for the variable delay SPE DD measurements for Snibson where the <sup>13</sup>C T<sub>1s</sub> were relatively short. In this case, up to ten dephasing periods in the range of 1 to 200  $\mu$ s were used before the first rotational modulation. However, for the other samples with <sup>13</sup>C T<sub>1s</sub> much longer than 5 s, a recycle time of either 100 or 120 s was used in the SPE DD experiment with, due to the sensitivity limitations, only a single delay of 60  $\mu$ s. In order to check that the tuning had remained virtually constant throughout the duration of all the DD experiments, the delays were arranged in a random order and between 1000 and 3000 scans were accumulated for each delay. No background signal was evident in the SPE spectra from the Kel-F rotor caps. All the FIDs were processed using a line broadening factor of either 50 or 100 Hz. The

Table 1 Analyses of the vitrinite concentrates

	Vitrinites					
	Snibson	Blidworth	Silkstone	Manton	Nantgarw	Oakdale
% moisture (ad)	8.9	4.1	13.4	4.0	1.1	1.5
% ash (dry basis)	2.7	1.6	1.3	1.1	2.4	7.8
% dmmf C	79.0	80.4	82.6	81.8	88.9	85.8
" " H	5.0	5.0	5.1	5.1	4.9	4.3
" " N	1.6	1.5	1.7	1.8	1.7	1.5
% Total S, dry basis	<0.3	<0.3	1.1	0.58	0.35	0.46
H/C ratio	0.76	0.75	0.74	0.74	0.66	0.61
Vitrinite reflectance, R <sub>o</sub> % av.	0.47	0.59	0.66	0.79	1.08	1.32
Maceral comp.						
Liptinite	7.6	8.0	7.4	9.0	0.4	2.0
% v/v Vitrinite	87.8	90.0	88.2	89.6	93.4	93.6
Inertinite	4.6	2.0	4.4	1.4	6.2	4.4

ad = as determined.

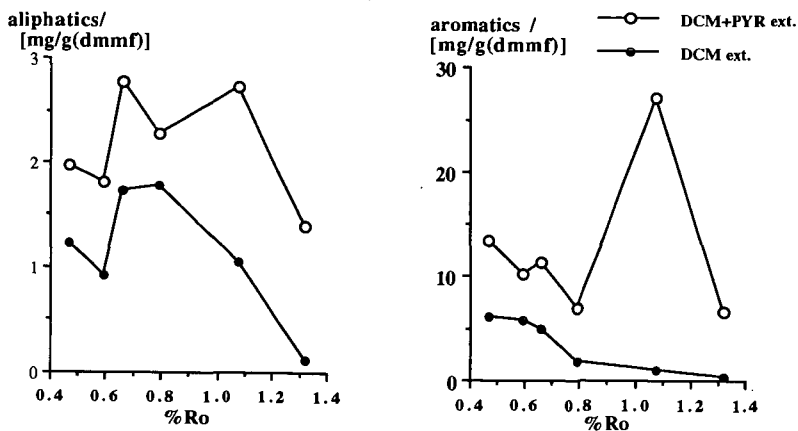


Figure 1 Yields of alkanes and aromatics from DCM and pyridine extraction stages as a function of vitrinite reflectance.

measurement of aromatic and aliphatic peak areas manually was found to be generally more precise than using the integrals generated by the spectrometer software.

## RESULTS AND DISCUSSION

**Fraction yields** Inspection of Figure 1 showing the yields of the total aliphatic and aromatic fractions recoverable with DCM and the cumulative yields following the subsequent pyridine reflux indicates that a substantial amount of low MW material is indeed clathrated within the vitrinite macromolecular structure across the rank range. Such material is contained in the closed pores of the vitrinite according to Radke et al.<sup>(24)</sup> and, as the rank increases, these will account for greater proportions of the decreasing overall pore volume. This explains the relatively large amounts of aromatic species which are accessible to pyridine but not to DCM extraction especially at higher rank. Aromatic species are more strongly retained than the alkanes (Figure 1) which would appear to be more easily forced through the pores and into the easily extractable bitumen. Nantgarw (%R<sub>o</sub> = 1.08) represents a maturity where the principal cracking reactions have occurred but, relatively, condensation of aromatic moieties is in its infancy giving rise to the highest yield of pyridine-extractable aromatics (Figure 1).

The yields of alkanes and aromatics in the range 0.1-0.5% (dmmf basis) from catalytic hydrogenation were comparable to those from pyridine extraction but did not vary systematically across the rank range. As anticipated, the hydrogenation yields for the vitrinites were considerably lower than those obtained previously for a Type I and a Type II kerogen due to the lower concentrations of labile C-O and C-S bonds<sup>(26)</sup>.

**Biomarker profiles** The various aliphatic and aromatic biomarker maturity parameters are listed in Table 2 which indicates that those for the DCM-extractable phase correlate to varying degrees with vitrinite reflectances. In particular, the following trends with increasing %R<sub>o</sub> can be noted.

- (i) The MPI increases and the calculated vitrinite reflectances are in remarkably good agreement with the actual values.
- (ii) The hopane C<sub>22</sub> and sterane C<sub>20</sub> S/S+R ratios are sensitive to changes in vitrinite reflectance before the oil-generating window (Stribson-Silksworth, %R<sub>o</sub> 0.47-0.66) with the sterane ratio extending somewhat further up to Manton.
- (iii) The C<sub>30</sub> β/αβ ratio decreases steadily with increasing rank.

These trends would hence appear to be representative of the geothermal stress experienced by the organic matter.

In the pyridine extracts the distribution of biomarkers with respect to their DCM counterparts would appear to be rank dependent. For the lowest rank members of the suite, Stribson and Blidworth, the aliphatic indices show a slightly more mature profile (Table 2) which could arise from the catalytic effects of the small amounts of minerals present<sup>(25)</sup> on an otherwise homogeneous distribution. Such material in intimate contact with the mineral matrix is often designated as the "bitumen 2" in oil shales and clays<sup>(26)</sup>. More interestingly at higher rank (Nantgarw and Oakdale), some components in the clathrated phase seem to represent those which have been more recently cleaved from the macromolecular framework. These are conspicuous by their relatively immature conformation (Table 2) having been preserved in the macromolecule by covalent bonding till release at higher maturity. For example, the higher MW members of the extended hopane series which are usually lost rapidly with thermal maturation are observed more prominently in the pyridine extractable alkanes than in those recovered by DCM treatment, even for the Oakdale vitrinite. In terms of detecting such immature biomarker distributions in the clathrated phase, Silkstone marks the cross-over point in this suite of samples. Although significant proportions of the biomarkers identified may well be derived from the small amounts of liptinite present (Table 1), it appears that their accessibility to solvents is governed by the changes in the bulk, i.e. vitrinite structure as a function of rank.

Table 2. Selected Aliphatic and Aromatic Biomarker Maturity Parameters

SAMPLE	STAGE	Aliphatics					Aromatics			
		C <sub>31</sub> αβ a	C <sub>32</sub> αβ b	C <sub>30</sub> c β/αβ	C <sub>27</sub> β/α d	T <sub>s</sub> / T <sub>m</sub> e	C <sub>29</sub> ααα f	MPI 1 g	%R <sub>c</sub> h	MPRI
Snibston	DCM	0.46	0.32	0.63	0.78	0.00	0.11	0.15	0.49	trace
	PYR	0.48	0.38	0.44	0.49	0.08	0.22	P	N.A.	trace
	HYD	0.30	0.24	1.03	0.67	0.00	0.22	P	N.A.	trace
Blidworth	DCM	0.60	0.55	0.46	0.09	0.00	0.36	0.34	0.60	1.04
	PYR	0.56	0.56	0.44	0.09	0.07	0.39	P	N.A.	trace
	HYD	0.40	0.42	0.47	0.29	0.11	0.26	P	N.A.	trace
Silkstone	DCM	0.58	0.57	0.37	0.07	0.03	0.43	0.41	0.65	1.10
	PYR	0.51	0.55	0.39	0.07	0.00	0.44	0.31	0.59	1.17
	HYD	0.52	0.52	0.40	0.23	0.13	0.36	0.16	0.50	trace
Manton	DCM	0.60	0.59	0.32	0.09	0.03	0.48	0.63	0.78	1.10
	PYR*	0.60	0.59	0.30	0.11	0.03	0.46	0.68	0.81	0.90
	DCM	0.56	0.51	0.13	0.30	0.74	0.48	1.07	1.05	2.15
Nangarw	PYR*	N.D.	N.D.	N.D.	N.D.	N.D.	N.D.	1.06	1.04	1.96
	HYD	0.51	0.54	0.36	0.91	0.63	0.37	1.11	1.07	1.91
	DCM	0.57	0.58	0.07	0.00	0.45	0.50	1.52	1.31	3.34
Oakdale	PYR	0.57	0.62	0.07	0.00	0.38	0.44	0.94	0.96	2.71

KEY

DCM = dichloromethane extraction, PYR = pyridine reflux, CAT = catalytic hydrogenation. (see experimental for details).  
 N.D. = Not determined. \* = not sequentially extracted. N.A. = Not available.  
 a: α,β - homothiophane 22S/ 22S+22R. Starting value 0, end value 0.5-0.6 (attained before oil generating period)  
 b: α,β - bishomothiophane 22S/ 22S+22R. Starting value 0, end value 0.5-0.6 (attained before oil generating period)  
 c: C<sub>30</sub> moretane/ α,β - hopane. In this rank range, the lower the value, the greater the maturity.  
 d: C<sub>27</sub> 17β(H)- 22, 29, 30-trisnorhopane / 17α(H)- 22, 29, 30-trisnorhopane. At lower ranks, higher values indicate low maturities.  
 e: C<sub>27</sub> 18α(H)- 22, 29, 30-trisnorhopane / 17α(H)- 22, 29, 30-trisnorhopane. At higher ranks, higher values indicate high maturities.  
 f: C<sub>29</sub> ααα - sterane 20S/ 20S+20R. Starting value 0, end value around 0.5. Extends further into the oil window than parameters (a) & (b).  
 g: MPI 1 = 1.5 ((2-MP)+[3-MP]) / ((P)+[1-MP]+[9-MP]) where [P] and [MP] denote phenanthrene and methylphenanthrene respectively.  
 h: 'P' in table indicates that the amount of phenanthrene detected far exceeded the concentrations of all methylphenanthrenes.  
 I: The predicted vitrinite reflectance from MPI 1, R<sub>c</sub>(%) = 0.60 MPI 1 + 0.40 (for MPR < 2.65)  
 I: MPR = [2-MP] / [1-MP], 'trace' indicates small, unresolvable contributions from all methylphenanthrenes.

The use of the sterane internal standards has indicated semi-quantitatively that the amounts of molecular (DCM- and pyridine-extractable) hopanes and steranes decrease markedly with increasing rank. However, this depletion is substantially less marked when one takes account of the significant amounts released by the hydrogenation step (see above).

Biomarkers such as C<sub>31</sub> and C<sub>32</sub> α,β-hopanes with the 22R configuration, C<sub>27</sub> 17β (H) - 22, 29, 30-trisnorhopane and C<sub>29</sub> (α,α,α-20R) steranes can be extracted from peats during early diagenesis (7) and all are detected in higher proportions than expected in the hydrogenation products, even for the highest rank of vitrinite (Nantgarw) to which this step has been applied (Table 2). This confirms that configurations can be preserved through incorporation of biolipids into the macromolecular structure during early diagenesis and this holds for both chiral centres which are part of a ring or in an alkyl sidechain.

**Carbon skeletal parameters** Table 3 summarises the carbon skeletal parameters obtained from the SPE <sup>13</sup>C NMR measurements. Due to the time consuming nature of these experiments, only results for 4 of the samples have been obtained thus far. As a check on the self-consistency of both the aromaticities and the non-protonated aromatic carbon concentrations obtained for the vitrinite concentrates, their aliphatic H/C ratios have been derived using the following relationship (23):

$$(H/C)_{\text{overall}} = (H/C)_{\text{ali}}(1 - f_a) + (H/C)_{\text{ar}}'f_a \quad (i)$$

where  $f_a$  is the aromaticity and  $(H/C)_{\text{ar}}'$  is the aromatic H/C ratio including phenolic hydrogen =  $(1 - C_{\text{np,ar}})/C_{\text{ar}}$ ,  $C_{\text{np,ar}}/C_{\text{ar}}$  being the fraction of non-protonated aromatic carbon corrected for phenols. For the bituminous coal samples, it has been assumed that the phenolic groups account for 60 % of the total oxygen consistent with much of the information in the literature (23).

Table 3 Carbon skeletal parameters derived from solid state <sup>13</sup>C SPE NMR spectroscopy

SAMPLE	$f_a$ (1)	$C_{\text{NP,AR}}/C$ (2)	$(H/C)_{\text{EL}}$ (3)	$(H/C)_{\text{AR}}^*$ (4)	$(H/C)_{\text{AL}}$ (5)
Snibston	0.77	0.46	0.76	0.40	1.8
Silkstone	0.79	0.52	0.74	0.34	2.0
Manton	0.81	0.53	0.74	0.35	2.1
Oakdale	0.87	0.53	0.61	0.40	2.1

**Key**

- (1): aromaticity, mole fraction of total sp<sup>2</sup> carbon.
- (2): mole fraction of non-protonated aromatic carbon over total carbon.
- (3): atomic H/C ratio derived from elemental analysis.
- (4): aromatic H/C ratio derived from (2), excluding phenolic OH.
- (5): aliphatic H/C derived by expression (i) in text.

The aliphatic H/C ratios derived using expression (i) are in the range, 1.8-2.1 (Table 3) which appears to be reasonably consistent with structural information derived from other techniques (23). The key finding is that, in the rank range from Snibston to Manton where %R<sub>o</sub> increases from 0.47 to 0.79 (Table 1), there is a small increase in carbon aromaticity (0.79 to 0.81), but the fractions of non-protonated carbon (0.52-0.53, Table 3) and the atomic H/C ratios (Table 1) remain constant. It is difficult to derive unambiguously the fraction of bridgehead aromatic carbons from the total fraction of non-protonated aromatic carbons since the fractions of alkyl and heteroatom-attached carbons must be subtracted and this is beyond the scope of this investigation. However, the relatively small variations in O content (by difference, Table 1) of ca 2% and the similarity of the aromaticities and fractions of non-protonated carbon (Table 3) would suggest that the proportions of

bridgehead aromatic carbon vary by no more than 3-5 mole % carbon. However, this still might be significant given that there is a change of 9 mole % in going from naphthalene to phenanthrene. Thus, although the degree of condensation of the aromatic structure is not likely to change markedly or to an extent that can readily be detected by solid state  $^{13}\text{C}$  NMR, it could well be that secondary factors, particularly the anisotropy of aromatic nuclei as reflected by the extent of non-covalent associative interactions are responsible for the variation in vitrinite reflectance.

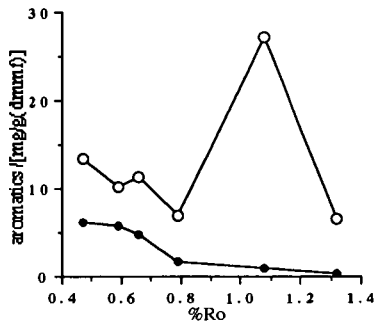
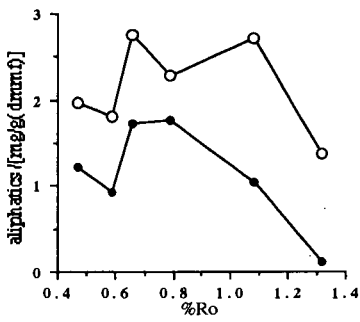
#### ACKNOWLEDGEMENTS

The authors thank the the Science and Engineering Research Council (Grant no.GR/F/87264) and British Gas plc (CASE studentship for GDL) for financial support.

#### REFERENCES

1. Fu J., Sheng G., Xu J., Eglinton G., Gowar A.P., Jia R., Fan S. and Peng P. (1989). In *Advances in Organic Geochemistry 1989* (Edited by Durand B. and Behar F.), *Org. Geochem.* **16**, 93-104, Pergamon Press, Oxford.
2. Chaffee A.L., Hoover D.S., Johns R.B. and Schweighardt F.K. (1986) *In Biological Markers in the Sedimentary Record* (Edited by Johns R.B.), pp. 311-345. Elsevier, Amsterdam.
3. Mackenzie A.S. (1984) In *Advances in Petroleum Geochemistry* (Edited by Brooks J and Welte D.), Vol 1, pp. 115-214. Academic Press, London.
4. Radke M., Welte D.H. and Willsch H.(1982) *Geochim. Cosmochim. Acta* **46**, 1-10.
5. Radke M., Willsch H., Leythaeuser D and Teichmuller M. (1982) *Geochim. Cosmochim. Acta.* **46**, 1831-1848.
6. Radke M. and Welte D.H. (1983) *In Advances in Organic Geochemistry 1983* (eds. M. Bjoroy et al.), pp. 504-512. Wiley.
7. Michaelis W., Richnow H.H., Jenisch A., Schulze T. and Mycke B. (1989) *In Facets of Modern Biogeochemistry* (Eds Itterkkot V., Kempe S., Michaelis W. and Spitzzy), pp 389-402, Springer Verlag, Heidelberg.
8. Mycke B. and Michaelis W. (1986) *In Advances in Organic Geochemistry 1985* (eds. Leythaeuser D and Rullkottter J.), *Org. Geochem.* **10**, 847-858. Pergamon Press, Oxford.
9. Hayatsu R., Winans R.E., Scott R.G., Moore L.P. and Studier M.H. (1978) *Fuel* **57**, 541-548.
10. Youtcheff J.S., Given P.H., Baset Z. and Sundaram M.S. (1983) *Org. Geochem.* **5**, 157-164.
11. Monthieux M. and Landais P. (1987) *Fuel* **66**, 1703-1708.
12. Green T.K. and Larsen J.W. (1984) *Fuel* **63**, 1538-1547.
13. Nishioka M. (1992) *Fuel* **71**, 941-948
14. Kuehn D.W., Davies A., Snyder R.W., Starsinic M., Painter P.C., Havens J. and Koenig J.L. (1982) *Prepr. Am. Chem. Soc. Div. Fuel Chem.* **27**, 55-63.
15. Furimsky E. and Ripmeester J. (1983) *Fuel Process. Technol.* **7**, 191-202.
16. Russell N.J., Wilson M.A., Pugmire R.J. and Grant D.M. (1983) *Fuel* **62**, 601-605.
17. Carr A.D. and Williamson J.E. (1990) *In Advances in Organic Geochemistry 1989* (eds. Durand B. and Behar F.), *Org. Geochem.* **16**, 313-323. Pergamon Press, Oxford.
18. Franz J.A., Garcia R., Linchan J.C., Love G.D. and Snape C.E. (1992) *Energy & Fuels* **6**, 598-602.
19. Love G.D., Snape C.E. and Carr A.D. (1991) *Proc. Int. Conf. on Coal Sci.* (Newcastle), 64-67.
20. Snape C.E. and Love G.D. (1991) *Prep. Am. Chem. Soc. Div. Fuel Chem.* **36(3)**, 877-883.
21. Larsen J.W. and Mohammadi M. (1990) *Energy & Fuels* **4**, 107-110.
22. Lafferty C.J., Mitchell S.C., Garcia R. and Snape C.E. (1993) *Fuel* **72**, 367-372.
23. Love G.D., Law R.V. and Snape C.E. (1993) *Energy & Fuels*, in press.
24. Radke M., Willsch H. and Teichmuller M. (1990) *Org. Geochem.* **15**, 539-563
25. Jovancicevic B., Vitorovic D. and Wehner H. (1992) *Org. Geochem.* **18**, 511-519.
26. Love G.D. and Snape C. E., unpublished work.

Figure 1 : Yields of aliphatic (left) and aromatic (right) fractions produced from dichloromethane extraction -●- and from dichloromethane then pyridine extraction (cumulative) ○- for the vitrinite suite.



## EFFECT OF CHLOROBENZENE PRE-TREATMENT ON MACROMOLECULAR STRUCTURE OF BITUMINOUS COALS

Carol A. McArthur, Peter J. Hall, Alexander J. MacKinnon and Colin E. Snape

University of Strathclyde, Dept. of Pure & Applied Chemistry, Thomas Graham  
Building, 295 Cathedral street, Glasgow G1 1XL, UK.

Keywords: Conformational changes, liquefaction

### ABSTRACT

Recent work has demonstrated that chlorobenzene (CB) pre-treatment can affect the mass transfer characteristics of Pittsburgh No.8 Argonne Premium Coal Sample (APCS), as indirectly it results in significantly altered product yields in a number of liquefaction regimes. Pre-treatment of Pittsburgh No.8 APCS with CB results in significant conformational changes and this is then reflected by examination with differential scanning calorimetry (DSC), surface area (SA) measurement and broadband  $^1\text{H}$  NMR relaxation. DSC reveals the existence of a glass to rubber transition ( $T_g$ ) for untreated and treated samples in the region 110°C to 120°C, with the transition shifted to a lower temperature for the CB treated coal.  $\text{CO}_2$  adsorption indicates that CB treatment markedly affects the amount of  $\text{CO}_2$  adsorbed and the equilibration behaviour. The chlorobenzene treatment caused the  $^1\text{H}$  thermal relaxation times to generally increase, in contrast to pyridine extraction where the reverse trend is usually observed.

### INTRODUCTION

It has been previously summarised that in cases where improved liquid product yields had been achieved in coal liquefaction<sup>(1-8)</sup>, the accessibility of solvents within the highly porous macromolecular structure of coals has been improved, particularly during the initial stages of liquefaction where retrogressive reactions need to be avoided. However, interpretation of these phenomena in terms of changes in the macromolecular structure of coals is complicated by the fact some organic matter is being removed at the same time that conformational changes may be occurring. Chlorobenzene has the advantage of extracting virtually no organic matter from coals. Further, it is non-polar and would not be expected to significantly disrupt hydrogen bonds at relatively low temperatures (<150°C) in coals.

It was found that the chlorobenzene treatment improved the oil yields (as measured by dichloromethane-solubles) in short contact time hydrogen-donor solvent liquefaction with tetralin (400°C, 15 min.) for the 3 bituminous coals<sup>(9,10)</sup>. As well as short contact time liquefaction with tetralin, improved oil yields were also achieved upon chlorobenzene treatment in solvent-free (dry) hydrogenation of Pittsburgh No. 8 coal<sup>(9)</sup>. The amounts of hydrogen transferred from the tetralin were broadly similar for the initial and chlorobenzene-treated coals strongly suggesting that the improved oil (DCM) yields arise from limiting retrogressive char-forming reactions rather than cleaving more bonds *per se*. However, the increased oil yields were accompanied by reductions in the overall conversions to pyridine-solubles for two out of the three bituminous coals investigated. Reducing the pre-treatment time from the standard 3 day period to 3 hours for Point of Ayr gave similar conversions with tetralin indicating that the conformational changes occur relatively fast, particularly in relation to the timescales of over 3 days usually associated with completely removing solvent-extractable material. This trend would appear to be consistent with the recent communication by Larsen and

co-workers<sup>(11)</sup> who found that the chlorobenzene treatment reduced the yield of pyridine-insolubles from tetralin extraction of the Illinois No. 6 APCS.

In the continuing investigation into the effects of chlorobenzene treatment on coal conversion phenomena, the effect of the pre-treatment on the macromolecular structure has been investigated using DSC, broadline <sup>1</sup>H NMR and CO<sub>2</sub> adsorption. Further liquefaction experiments have been conducted using hydrogenated anthracene oil and solvent free hydrogenation. Point of Ayr coal under relatively low temperature pyrolysis was conducted to ascertain whether the same effect occurred as pre-treating with chlorobenzene.

### **EXPERIMENTAL**

The standard chlorobenzene treatment of 3 days was applied to the coal samples of Point of Ayr (87% dmmf C), Bentineck (83% dmmf C) both of which are UK coals and Pittsburgh No. 8 APCS. As previously described with tetralin, extractions with HAO and hydroliquefaction with naphthalene were conducted with a solvent to coal mass ratio of 2:1 and contact times of 15 and 60 min. at 400°C, yields of DCM- and pyridine-insolubles being determined. Pyrolysis of Point of Ayr was conducted in a tube furnace. The sample was heated up to 180°C at a rate of 5°C min<sup>-1</sup> under nitrogen then cooled to room temperature, the volatile matter property was then compared to that of the CB treated coal.

DSC was carried out on the initial and chlorobenzene-treated samples of the Pittsburgh No. 8 APCS using a Mettler DSC 30 system. The standard aluminum pan used contained two holes which allowed the evaporation of water. Each sample was weighed into the aluminum pan and then dried under a stream of nitrogen at 110°C before being cooled to 30°C and reweighed. DSC was then performed by heating the sample at 10°C min<sup>-1</sup> to 250°C.

<sup>1</sup>H NMR thermal relaxation times (T<sub>1</sub>s) were determined at 100 MHz using the Bruker MSL 100 spectrometer by inversion recovery using single point acquisition for the free induction decays. 128 delays were used with fixed increments of either 6 or 10 ms. The data were fitted either to a single or two components using the SIMFIT Pascal programme; the smaller increment of 6 ms gave more data points covering the initial relaxation and this favoured a two component fit.

To determine the effects of chlorobenzene treatment on rates of mass transfer, CO<sub>2</sub> adsorption at 19K and a P/P<sub>0</sub> of 0.05 was measured using a Quantasorb Quantachrome instrument.

### **RESULTS AND DISCUSSION**

#### **Volatile Matter**

Table 1 shows the volatile matters for initial coal, chlorobenzene treated coal and the pyrolysed coal (180°C). The value has remained within experimental error indicating that the volatile matter has not been altered during either of the treatments. Therefore any change in yields for the CB treated coal can be accounted for by a change in the macromolecular structure.

### Hydrogenated anthracene oil extractions

The yields obtained from the initial and chlorobenzene-treated samples of Point of Ayr and Bentinck coals with residence time of 60 min. are summarised in Table 2. The effects of the pretreatment on conversions are relatively small for Point of Ayr coal, especially compared with tetralin<sup>(9,10)</sup>. In contrast, significant reduced overall conversions to pyridine-solubles have been obtained for Bentinck coal with a concomitant reduction in oil yield at the longer residence time (Table 2).

HAO is largely in the liquid phase at 400°C and, intuitively, should be affected less by conformational changes brought about by the chlorobenzene treatment than smaller molecules in the vapour phase, such as tetralin. Nonetheless, mass transport phenomena would still appear to be affected, particularly for Bentinck where the ability of HAO to prevent retrogressive reactions has been curtailed.

### Batchwise hydrogenation

Table 3 lists the conversions obtained for Bentinck coal. In contrast to Pittsburgh No.8 coal<sup>(9)</sup>, a reduced yield of DCM-soluble products was obtained upon treatment which would appear to be consistent with the general trend reported above in naphthalene hydroliquefaction. This presents further evidence that the effects of the chlorobenzene-treatment on the liquefaction behaviour of Bentinck are markedly different to those for Pittsburgh No.8 and Point of Ayr coals.

### Naphthalene hydroliquefaction

The trends in naphthalene hydroliquefaction (70 bar cold hydrogen pressure) mirror those observed in the previous thermolytic extraction (Table 4) although the conversions to DCM-solubles are considerably higher due to the hydrogen over-pressure. For Point of Ayr coal, a small increase in the DCM-soluble product yield was obtained whereas, in contrast for Bentinck, there was a reduced overall conversion to pyridine-solubles (Table 4).

### Differential Scanning Calorimetry

The traces from the first 3 cycles of the experiments in which initial and chlorobenzene-treated Pittsburgh No.8 coal were heated and cooled repeatedly are shown in Figure 1. The initial coal displays a broad feature centred at *ca* 145°C but, after heating to 250°C, this shifts irreversibly to much lower temperature (105-115°C) where it becomes truly reversible; the traces for the second and all subsequent heating cycles are virtually identical (Figure 1) and hence the event is characteristic of a glass to rubber transition. This behaviour was also recently reported by Mackinnon and Hall for the Illinois No.6 APCS<sup>(12)</sup> and is broadly similar to that for many polymer systems which first of all undergo an initial enthalpy relaxation before displaying reversible glass to rubber transitions.

After chlorobenzene treatment, the initial irreversible transition observed for the parent coal is no longer present. The trace comprises a broad endotherm below 120°C which might be due to the evaporation of a small amount of residual solvent and a much sharper feature at 140°C. Upon subsequent heating, these features disappear and the traces obtained resemble those for the initial coal except the reversible glass to rubber transition has shifted *ca* 10°C lower (Figure 1).

This evidence confirms that chlorobenzene treatment has altered the conformation of the coal but, as for the initial coal, the treated coal then itself undergoes a further

irreversible change upon heating. The final conformation obtained may be somewhat different than that derived from the initial coal because of the lower reversible glass to rubber transition temperature.

### Broadline $^1\text{H NMR}$

Table 5 lists the  $^1\text{H T}_1$ s for the 3 bituminous coals before and after chlorobenzene treatment. The thermal relaxation behaviour of the Pittsburgh No.8 APCS was best fitted to two components. Upon treatment, there is a significant increase in  $^1\text{H T}_1$ s for Pittsburgh No. 8 (for the slower relaxing dominant component) and Point of Ayr coals but not for Bentinck. It is interesting to note that upon pyridine extraction, there is usually a marked reduction in  $^1\text{H T}_1$ s probably due to a combination of removing molecular species and the formation of new non-covalent (hydrogen-bonded) cross-links. However, upon prolonged vacuum drying, it has been found that the increase again implying that only a small amount of pyridine imbibed is required to significantly reduce the segmental motions (frequencies in the MHz range) within the macromolecular structure. Thus, the implication is that the chlorobenzene treatment has increased the mobility (possibly through the irreversible cleavage of non-covalent cross-links) within the macromolecular structure of two out of the three bituminous coals investigated.

### $\text{CO}_2$ Adsorption

Following CB treatment Pittsburgh No.8 and Point of Ayr showed an increase in the equilibrium uptake of  $\text{CO}_2$ . The relative increase for Pittsburgh No.8 was 1.77 and for Point of Ayr 1.43. These results are difficult to interpret unequivocally but it is known that  $\text{CO}_2$  swells coals at high pressures. Therefore, the increase in  $\text{CO}_2$  uptakes may indicate an increased propensity to swell in  $\text{CO}_2$ , which may increase accessibility. Whatever the correct explanation may be, this may have important consequences for the accessibility of other materials important to liquefaction. Kinetically, the adsorption of  $\text{CO}_2$  could be resolved into two distinct components: an initial rapid uptake was followed by a slower but more linear approach to equilibrium. After treatment, the exponential uptake proceeded more rapidly but the linear uptake region was not affected. This description extends the earlier data reported by PJH for Upper Freeport coal <sup>(13)</sup> in showing that both the amount adsorbed and equilibration behaviour are markedly affected by chlorobenzene treatment. We have attempted to model the uptake by a number of diffusion models but with no success, this may indicate mixed modes of diffusion occurring concurrently.

### General Discussion

It is now evident from the wide range of liquefaction experiments conducted on the 3 bituminous coals investigated that chlorobenzene treatment profoundly affects behaviour. Further, conversions are affected both as a function of both the liquefaction regime and the coal used. These findings imply that the conformational changes brought about by the treatment are not uniform and consequently the transport properties of reactants (i.e. solvents and hydrogen gas) in and products out of reacting coals are affected in different ways.

DSC, broadline  $^1\text{H NMR}$  and  $\text{CO}_2$  adsorption have all detected changes with DSC indicating that the initial and chlorobenzene-treated coals undergo irreversible but different transformations in the temperature range 130-150°C. Further, DSC has raised the issue as to how the effects of chlorobenzene and, indeed other solvent treatments, might differ than those brought about by simple heat-treatment. Other techniques that

can be used to probe these phenomena include small-angle X-ray scattering (SAXS), mechanical tests and simple swelling measurements. Yun and Suuburg have recently used dynamic mechanical analysis (DMA) to detect irreversible conformational changes brought about mild heating of the Pittsburgh No.8 and Upper Freeport APCS with the results being compared with DSC and solvent swelling<sup>(14,15)</sup>. They argue that DMA measurements are considerably more sensitive than DSC below 100°C for detecting changes induced by the removal of moisture with a transition at 60°C being observed for Pittsburgh No.8 coal. However, the events observed after heating the initial coal to 200°C do not appear to correspond to those found here by DSC for CB treatment.

#### ACKNOWLEDGEMENT

The authors thank the British Coal Utilisation Research Association (Contract No. B18) for financial support and Mr. G.D. Love for carrying out the <sup>1</sup>H NMR measurements.

#### REFERENCES

1. C.E. Snape, F.J. Derbyshire, H.P. Stephens, R.J. Kottenstette and N.W. Smith, *Fuel Process. Technol.*, 1990, **24**, 119.
2. A.K. Saini, C. Song and H.H. Schobert, *Prepr. Am. Chem. Soc. Div. Fuel Chem.*, 1993, **38(2)**, 593 and 601.
3. K.S. Vorres, D.L. Wertz, V. Malhotra, Y. Dang, J.T. Joseph and R. Fisher, *Fuel*, 1992, **71**, 1047.
4. M.A. Serio, P.R. Solomon, E. Kroo, R. Basilakis, R. Malhotra and D. McMillen, *Proc. 1991 Int. Conf. on Coal Sci.*, p 656.
5. M.A. Serio, E. Kroo, H. Teng and P.R. Solomon, *Prepr. Am. Chem. Soc. Div. Fuel Chem.*, 1993, **38(2)**, 577.
6. J.T. Joseph and T.R. Forrai, *Fuel*, 1992, **71**, 75.
7. K. Shams, R.L. Miller and R.M. Baldwin, *Fuel*, 1992, **71**, 1015.
8. S. Kelkar, K. Shams, R.L. Miller and R.M. Baldwin, *Prepr. Am. Chem. Soc. Div. Fuel Chem.*, 1993, **38(2)**, 554.
9. C.A. McArthur, A.J. MacKinnon, P.J. Hall and C.E. Snape, *Prepr. Am. Chem. Soc. Div. Fuel Chem.*, 1992, **37** (San Francisco meeting).
10. C.A. McArthur, P.J. Hall and C.E. Snape, *Prepr. Am. Chem. Soc. Div. Fuel Chem.*, 1993, **38(2)**, 565.
11. J.W. Larsen, M. Azik and A. Korda, *Energy & Fuels*, 1992, **6**, 109.
12. A.J. Mackinnon and P.J. Hall, *Fuel*, 1992, **71**, 974.
13. P.J. Hall and J.W. Larsen, *Energy and Fuels*, 1991, **5**, 228.
14. Y. Yun and E.M. Suuberg, *Energy & Fuels*, 1992, **6**, 328.
15. Y. Yun and E.M. Suuberg, *Prepr. Am. Chem. Soc. Div. Fuel Chem.*, 1993, **38(2)**, 491.

**Table 1 Volatile Matter for the Point of Ayr Samples**

	%daf coal % V.M
Initial coal	30.0
CB-treated coal	31.3
Pyrolysed coal	29.5

**Table 2 Hydrogenated Anthracene Oil Extractions with a Contact Time of 1 Hour**

	%DCM conv.*	%daf coal	
		%Pyr-sols/DCM-insols	% Pyr-insols
<b>Point of Ayr (a)</b>			
Initial coal	39.6	39.9	20.5
CB treated coal	38.9	43.5	17.6
<b>Bentinck (a)</b>			
Initial coal	54.1	42.3	3.6
CB treated coal	40.8	41.9	17.3

**Table 3 Hydrogenation of Bentinck Coal (1 Hour Residence Time)**

	%DCM conv.*	%daf coal	
		%Pyr-sols/DCM-insols	% Pyr-insols
Initial coal (a)	22.2	22.6	55.2
CB-treated coal (a)	12.9	31.9	55.2

**Table 4 Hydroliquefaction using Naphthalene (1 Hour Residence Time)**

Coal	%DCM conv.*	% daf coal	
		%Pyr-sols/DCM-insols	% Pyr-insols
<b>Point of Ayr (a)</b>			
Initial coal	29.3	36.8	33.9
CB treated coal	35.4	28.3	36.3
<b>Bentinck (a)</b>			
Initial coal	27.3	31.2	41.5
CB treated coal	27.9	19.0	53.1

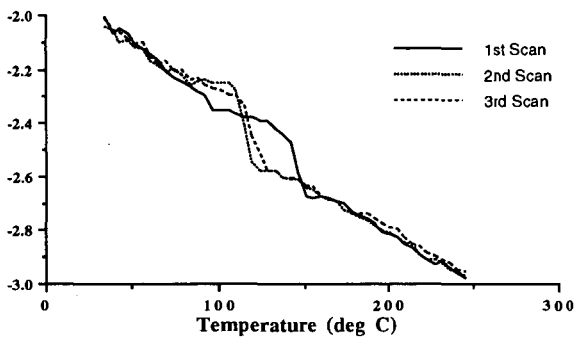
\* = 100 - % DCM-insols, includes DCM soluble liquid product + gas + water.

(a) = mean of duplicate runs.

**Table 5 <sup>1</sup>H Thermal Relaxation Times (T<sub>1s</sub>) for Initial and Chlorobenzene-Treated Coals**

Coal	T <sub>1s</sub> , ms	
	Initial	CB-treated
Pittsburgh No.8	176 (82%)	198 (72%)
	7.3 (18%)	7.3 (28%)
Point of Ayr	76 (100%)	109 (100%)
Bentinck	90 (100%)	89 (100%)

Heat flow (mW) Untreated Pittsburgh No.8



Heat Flow (mW) Chlorobenzene treated Pittsburgh No.8

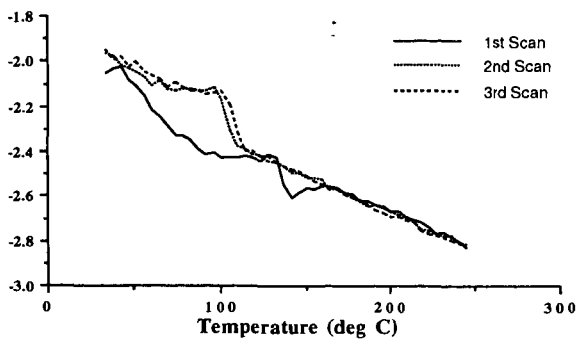


FIGURE 1 DSC ANALYSIS OF PITTSBURGH No.8 COAL

## NATURE OF CROSS-LINK BONDS FOR SOME BITUMINOUS COAL

M. Iino, H.-T. Liu, T. Ishizuka,  
M. Fujiwara, and T. Takanohashi  
Institute for Chemical Reaction Science,  
Tohoku University, Katahira 2-1-1, Aoba-Ku  
Sendai 980, Japan

Keywords: Coal structure, One-Component Model, Solvent Extraction.

### INTRODUCTION

The two-component (phase) model of coal structure, in which coal consists of two components, i.e., a macromolecular, covalently cross-linked network and a relatively low molecular weight, molecular component trapped inside the network, seems to be widely accepted, from NMR relaxation(1) pyrolysis(2), and catalytic hydrogenation(3) studies for bituminous coals, and from liquefaction study(4) for low-rank coals. Nishioka(5), however, suggests that one-component model, in which coal consists of one component of physically associated molecules, i.e., aggregates of coal molecules of various molecular weight, is more suitable for some bituminous coals.

In this paper structure model of bituminous coals, especially nature of bonds which form a cross-linked network, is discussed from our results, including the results already published(6-13), about the extraction of coals with CS<sub>2</sub>-N-methyl-2-pyrrolidinone (NMP) mixed solvent and characterization of the extracts and residues obtained with the mixed solvent.

### EXPERIMENTAL

Extraction and fractionation procedures are shown in Figure 1. The coals were exhaustively extracted with CS<sub>2</sub>-NMP mixed solvent(1:1 by volume) at room temperature under ultrasonic irradiation, according to the method described before(6,11). The solubility of the extract fractions was determined from the amount of the insoluble part when 400mg of the sample in 50ml of the CS<sub>2</sub>-NMP mixed solvent was ultrasonically irradiated for 30min at room temperature, in the presence or absence of an additive(9). The swelling ratio(Q) was measured by the volumetric method(14).

### RESULTS AND DISCUSSION

#### Extraction Yield with the CS<sub>2</sub>-NMP Mixed Solvent

The two-component model assumes the existence of a large amount of

covalently cross-linked network which is not soluble, i.e., which is not extracted with any solvents. In fact, the extraction yields higher than 40wt%(daf) are hardly obtained so far without covalent bond breaking in coal. CS<sub>2</sub>-NMP mixed solvent(1:1 by volume), however, was found to give very high extraction yields at room temperature. Table 1 shows the extraction yields with the mixed solvent for the coals which gave the yield higher than 40wt%(6). ZZ(China), SY(Japan), and UF(USA) coals gave the yields higher than 50wt%. Another ZZ coal, which was obtained recently, gave 77.9wt% of the extraction yield(10). No solubilization reactions in the mixed solvent extraction, such as covalent bond breaking, is suggested from several experimental results including characterization of the extracts and residues obtained. One of the important results supporting the conclusion above is that the heavier fraction than preasphaltene, i.e., the pyridine insoluble extract fraction, could be obtained by this extraction.

Table 2 shows the effect of TCNE addition on the extraction yield with the CS<sub>2</sub>-NMP mixed solvent. UF(Argonne sample) coal increased the extraction yield from 60.4wt% to 85.0wt%, and UF-P(PSOC sample), LK, and SG coals gave the yield higher than 50wt%, by the addition of TCNE. The effect of TCNE can be explained by the breaking of associations between coal molecules by TCNE, as described in the last section, not by the breaking of covalent bonds in coal. This indicates that UF coal, for example, have 85wt% of solvent soluble component.

The extracts swell in the solvent which does not dissolve them, suggesting that they have a kind of a cross-linked structure(12). Since an extract is soluble in the extraction solvent and cross-linked network consisting of covalent bonds is insoluble in any solvent, the extracts, which was obtained here with the high yields, seem to be a giant assembly(aggregate) of a small molecules by noncovalent bonds such as hydrogen bonds and charge transfer interaction.

#### Similarity of the Extract and Residue. Continuity of Coal Structure

Figure 2(7) shows the fraction distribution of E-AS, E-PS, E-PI, and residue, which were obtained from the extraction with the CS<sub>2</sub>-NMP mixed solvent and subsequent fractionation. Table 3(7) shows that the values of ultimate analysis of each fractions are similar, or gradually increase or decrease with the order of E-AS, E-PS, E-PI, and residue. No clear discontinuity was found between E-PI and residue. VM(daf) in proximate analysis of the extracts(E-PS + E-PI) and residues were found to be very similar(7). Similar swelling ratios(Q) of E-PI and the residues in methanol, benzene, and THF for ZZ, SY, and LK coals were also obtained(12).

The results above that there is no discontinuity between the extract fraction and the corresponding residue suggest that one-component model is more suitable than two-component model, in which coal consists of two quite different components, for some bituminous coals used here.

#### Association of Coal Molecules

Coals have several kinds of noncovalent interactions such as hydrogen bonding, charge transfer, aromatic( $\pi$ )-aromatic( $\pi$ ), and dipole(ion)-dipole(ion) interaction, which varies depending on coal rank. E-PI from ZZ coal was found to become partly insoluble in the CS<sub>2</sub>-NMP mixed solvent due to the association of coal molecules and the addition of the separated lighter fractions, i.e., E-AS and E-PS, or other compounds such as TCNE and p-phenylenediamine(PDA) recovered its solubility in the mixed solvent(9), probably due to the breaking of the association of coal molecules by the additive. Similar result was obtained for E-PI from UF coal, i.e., the addition of only 0.025(g/g coal) of TCNE and PDA increased the solubility of E-PI in the mixed solvent from 55.1wt% to 99.0 and 96.5wt%, respectively.

Figure 3 shows IR spectra of the mixed solvent insoluble E-PI(E-PI-I) and soluble E-PI(E-PI-S(a)) fractions after TCNE treatment and E-PI-S after washing with benzene(b), THF(c), DMSO(d), and pyridine(e), respectively. Figure 3 shows that TCNE retained in E-PI-S was removed by better solvents than acetone(E-PI-S(a)) for coal molecules. Thus, the order of the degree of the TCNE removal, i.e., acetone < benzene < THF < DMSO < pyridine, agrees with that of the extraction yields obtained in the extraction with these solvents. The result that TCNE can be removed by solvent washing suggests that TCNE is retained by adsorption to PI due to noncovalent interactions, not by some chemical reactions such as Diels-Alder reactions.

#### CONCLUSIONS

High extraction yields obtained by using the CS<sub>2</sub>-NMP mixed solvent, similarity between the extracts and residues, and association and dissociation behavior coal molecules of coal molecules suggest that some bituminous coals such as UF and ZZ coals have coal structure in which coals consist of one component of a giant assembly (aggregates) of relatively small molecules. Covalently bonded cross-linked network, which is assumed in two-component model of coal structure, does not seem to be a main structure for these coals.

## REFERENCES

1. Jurkiewicz, A., Marzec, A. and Idziak, S. Fuel, 1981, 60, 1167.
2. Meuzelaar, H-L.C., Yun, Y., Simmleit, N. and Schulten, H. Am.Chem.Soc.Div.Fuel Chem.Prepr., 1989, 34(3), 693.
3. Derbyshire, F., Davis, A. and Lin R. Am.Chem.Soc.Div.Fuel Chem.Prepr., 1989, 34(3), 676.
4. Redlich, P., Jackson, W.R. and Larkins, F.P. Fuel, 1985, 64, 1383.
5. Nishioka, M. Fuel, 1992, 71, 941.
6. Iino, M., Takanohashi, T., Ohsuga, H. and Toda, K. Fuel, 1988, 67, 1639.
7. Iino, M., Takanohashi, T., Obara, S., Tsueta, H. and Sanokawa, Y. Fuel, 1989, 68, 1588.
8. Takanohashi, T. and Iino, M. Energy Fuels, 1990, 4, 452.
9. Sanokawa, Y., Takanohashi, T. and Iino, M. Fuel, 1990, 69, 1577.
10. Iino, M., Takanohashi, T., Ohkawa, T. and Yanagida, T. Fuel, 1991, 70, 1236.
11. Takanohashi, T. and Iino, M. Energy Fuels, 1991, 5, 708.
12. Fujiwara, M., Ohsuga, H., Takanohashi, T. and Iino, M. Energy Fuels, 1992, 6, 859.
13. Ishizuka, T., Takanohashi, T., Ito, O. and Iino, M. Fuel, 1993, 72, 579.
14. Green, T. K. and Larsen, J.W. Fuel, 1984, 63, 935.

Table 1. The selected<sup>a</sup> extraction yields with the CS<sub>2</sub>-NMP mixed solvent<sup>b</sup>

Coal	Symbol	Specification	Country	C% (daf)	Extraction yield (wt%, daf)
Zao Zhuang	ZZ	————	China	86.9	65.6
Shan Jia Ling	SJ	————	China	86.8	45.4
Shin-yubari	SY	————	Japan	86.7	60.6
Upper Freeport	UF	Argonne	USA	86.2	54.0
Ding Tian	DT	————	China	86.0	46.6
Ping Ding Shan	PS	————	China	85.4	43.0
Thurston Property	TP	SBN	USA	84.9	45.4
Lower Kittanning	LK	PSOC815	USA	84.0	46.8
Lingan	LG	SBN	Canada	83.6	41.2
Pittsburgh No.8	PB	Argonne	USA	82.6	40.1

<sup>a</sup>The yields higher than 40wt%(daf) were selected. <sup>b</sup>1:1 By volume.

Table 2. Effect of TCNE addition on the extraction of various coals with the CS<sub>2</sub>-NMP mixed solvent

Coal	C% (daf)	Amount of TCNE (g/g coal)	Extraction yield (wt%, daf)
SW	88.4	none	37.9
(Swell B)		0.100	47.9
UF	86.2	none	60.4
		0.025	85.0
UF-P*	85.0	none	44.2
		0.100	50.1
LK	84.0	none	46.2
		0.100	61.5
PB	82.6	none	39.0
		0.025	42.6
SG	77.8	none	37.5
(Stigler)		0.100	52.3

\*UF coal from PSOC.

Table 3. Ultimate analyses of the raw coals, extract fractions and residues

	Extract			Residue	Raw coal
	E-AS	E-PS	E-PI		
Zao Zhuang					
C	89.1	85.9	85.5	85.3	86.9
H	6.8	5.3	5.1	4.7	5.1
N	1.2	1.7	1.8	1.6	1.5
S	1.1	1.8	1.7	2.1	1.6
O*	1.8	5.3	5.9	6.3	4.9
H/C	0.91	0.74	0.71	0.66	0.70
O/C	0.015	0.046	0.052	0.055	0.042
Upper Freeport					
C	88.5	86.6	85.8	81.7	86.2
H	6.7	5.4	5.0	4.7	5.1
N	1.1	1.8	2.1	1.8	1.9
S	0.5	1.0	1.1	5.5	2.2
O*	3.2	5.2	6.0	6.3	4.6
H/C	0.91	0.75	0.70	0.69	0.71
O/C	0.027	0.045	0.052	0.058	0.040
Lower Kittanning					
C	86.4	84.7	83.4	79.9	82.3
H	6.7	5.3	5.1	4.9	5.2
N	1.1	1.9	2.1	1.6	1.7
S	1.1	1.3	1.2	5.0	3.9
O*	4.7	6.8	8.2	8.6	6.9
H/C	0.92	0.75	0.73	0.73	0.75
O/C	0.041	0.060	0.074	0.081	0.063

\*By difference

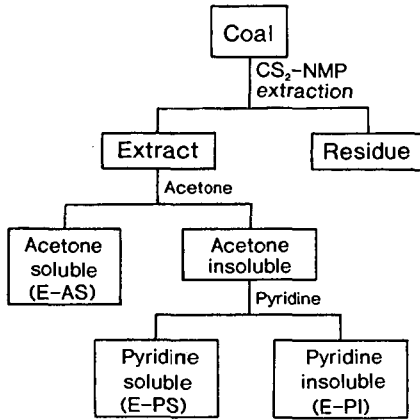


Figure 1. Solvent fractionation procedure of the extract obtained from the CS<sub>2</sub>-NMP mixed solvent extraction.

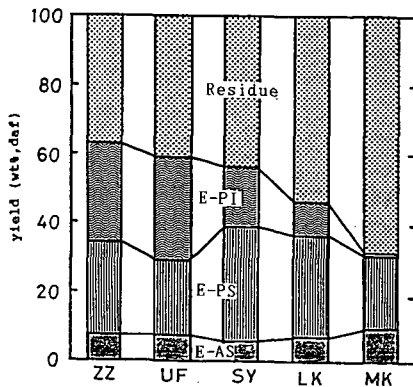


Figure 2. Fraction distribution for ZZ, UF, SY, LK and Miike(MK) coals

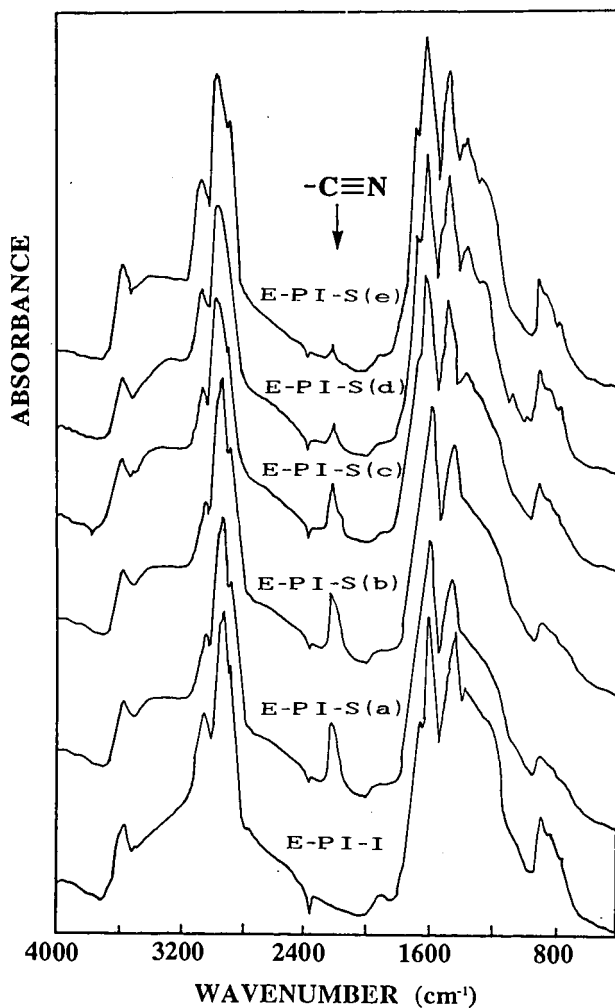


Figure 3. FT-IR spectra of the mixed solvent insoluble E-PI (E-PI-I) and soluble E-PI (E-PI-S(a)) fractions after TCNE treatment and E-PI-S after washing with benzene (b), THF(c), DMSO(d), and pyridine(e), respectively.

## A NEW MODEL FOR THE SWELLING OF COAL

Paul C. Painter and Suresh L. Shenoy  
Polymer Science Program  
Penn State University  
University Park, PA 16802

Key Words: Coal swelling, molecular weight, hydrogen bonding

### INTRODUCTION

Most studies of the swelling of coal have been based on the Flory-Rehner model for the swelling of polymer networks, sometimes modified to account for factors such as finite chain length, or in work conducted in this laboratory, hydrogen bonding interactions. However, as a result of work reported over the last ten years or so (e.g., references 1-5) it is now clear that there is a big problem with this approach. Although some data has been interpreted so as to bring in to question the fundamental assumption of the separability of the elastic and free energies (6,7), the most serious deficiency appears to be the second major assumption of the Flory-Rehner theory, that the deformation of the elementary chains of the network is in some fashion affine with the macroscopic deformation (swelling) of the sample. The neutron scattering work of Bastide et al. (3) has demonstrated that the network elementary chains have approximately the same dimensions as equivalent non cross-linked chains in solutions of the same concentration, which is much less than would be expected on the basis of an affine deformation model. These results are in good agreement with the  $c^*$  theorem of de Gennes (8), who proposed that in a good solvent the swollen coils of the network largely exclude one another from a volume that is (more-or-less) defined by their radius of gyration, but because the chains are forced into contact at their cross-link points the gel is analogous to the situation at the overlap threshold in a semi-dilute solution. Accordingly, Bastide et al. (2) proposed that the swelling of a gel proceeds by a process of topological rearrangement or disinterspersion of the cross-link points or nodules and demonstrated that an analysis based on a scaling approach is in good agreement with experimental observations.

In recent work we have modified the classical Flory-Rehner approach by abandoning the affine assumption (9). We have used the packing conditions that are a consequence of the  $c^*$  theorem and a scaling law to define a relationship between the degree of swelling and elementary chain extension. The model appears to provide a good description of various swelling and deswelling experiments and provides a simple foundation on which we can examine the swelling of coal. We can only report here an outline of the model and the theory will be presented in greater detail in a separate publication. We will consider first the basic equations for the free energy, then consider how these must be modified to account for two crucial features of coal structure, hydrogen bonding and finite chain length.

### THEORY AND CALCULATIONS

We start with a hypothetical perfect network of very long chains, each of the same length (degree of polymerization,  $N$ ) and cross-link functionality ( $f$ ). The treatment for equilibrium swelling in a good solvent where the swollen chains are at the threshold between the dilute and semi-dilute regimes is straightforward and uses three basic and familiar assumptions:

- 1) The free energy of the gel can be written as the sum of two separate components, describing the elastic free energy and mixing free energy, respectively.
- 2) These components of the free energy can be expressed in terms of the classic elastic free energy and the Flory-Huggins theory (modified later to account for hydrogen bonding).
- 3) Following de Gennes, we assume that *at equilibrium in a good solvent* the chains expand to the extent that they would in a dilute solution of the same solvent. The cross link points

disintersperse to the extent that the gel is a collection of spheres of individual network chains that as far as possible exclude segments of other chains from their volume, but are forced into contact at their cross-link points, as illustrated in figure 1.

Using the first two assumptions the equations for the free energy can be written down immediately, while the final assumption provides the essential connection between the volume fraction of polymer segments (i.e., the degree of swelling) and the chain expansion factor (9). The free energy is then given by:

$$\frac{\Delta F}{RT} = v \left[ \frac{3}{2} (\alpha^2 - 1) - \ln \alpha^3 \right] - \xi \ln \phi_c + n_s \ln (1 - \phi_c) + n_s \phi_c \chi \quad (1)$$

where  $n_s$  is the number of moles of solvent,  $\phi_s$ ,  $\phi_c$  are the volume fractions of coal and solvent, respectively  $\xi$  is the cycle rank of the network,  $v$  is the number of chains,  $\chi$  is the Flory-Huggins interaction parameter and  $\alpha$  is the chain expansion factor. The chemical potential of the solvent then follows immediately as:

$$\frac{\Delta \mu_s}{RT} = - \left[ 3v \left( \alpha - \frac{1}{\alpha} \right) \frac{\phi_c^2}{Nv} \right] \frac{\partial \alpha}{\partial \phi_c} + \frac{\xi \phi_c}{Nv} + \ln (1 - \phi_c) + \phi_c + \phi_c^2 \chi \quad (2)$$

In models that assume an affine deformation an expression for  $\partial \alpha / \partial \phi_c$  is obtained from the condition  $\phi_c = 1/\alpha^3$ . In using the  $c^*$  model we can obtain a similar relationship from the packing condition (9):

$$\phi_c' = \frac{1}{\alpha^3 N^{1/2}} \quad (3)$$

where  $\phi_c'$  is the volume fraction of coal segments within *each excluded volume domain* or "blob". For highly swollen networks  $\phi_c'$  is not the same as the overall or nominal concentration  $\phi_c$ , but we have calculated that for degrees of swelling less than 5 the packing factor that connects these two quantities is about 1 (9), so for coal, where the degrees of swelling are usually of the order of 2-3 we obtain

$$\frac{\Delta \mu_s}{RT} = \frac{\phi_c^{1/3}}{N^{4/3}} - \left( 1 - \frac{\xi}{v} \right) \frac{\phi_c}{N} + \ln (1 - \phi_c) + \phi_c + \phi_c^2 \chi \quad (4)$$

This is very similar in form to the Flory-Rehner result, differing only in the first term, where the assumption of an affine deformation results in a  $\phi_c^{1/3}/N$  term.

#### THE EFFECT OF HYDROGEN BONDING AND FINITE CHAIN LENGTH

The method we have used to describe hydrogen bonding interactions depends upon the determination of the modification to the number of configurations available to the chains when they are required to form their equilibrium distribution of hydrogen bonds, relative to the state where the chains are not hydrogen bonded at all. The details of this procedure have been presented elsewhere (10,11) and its initial application to coal has also been discussed (12). We will not reproduce the equations here but simply note that this introduces an extra term,  $\Delta \mu_H/RT$ , into equation 4, where the contributions of hydrogen bonds to the solvent chemical potential can be calculated from equilibrium constants that, in turn, can be experimentally determined using infrared spectroscopy (11).

The effect of finite chain length is less easily handled. Previously we used a model developed by Kovac (13) and first applied to coal by Larsen et al. (14). Here we will confine our calculations to a simpler approach. Flory (15) compared approximate distribution functions to an exact expression and

found for short chains (e.g.,  $N=4$ ) at small extensions the Gaussian function was the best approximation, but at higher extensions an inverse Langevin distribution (which Flory preferred to call the  $L^*$  distribution) was superior. In initial calculations we have found that strong specific interactions are a strong driving force for chain expansion, so we will employ both approximations and compare the results. In the Gaussian approximation we employ equation 4 with the added hydrogen bonding contribution, while the use of the  $L^*$  distribution gives:

$$\begin{aligned} \frac{\Delta\mu_z}{RT} = & \left[ 1 + \frac{3}{5}\alpha^2 + \frac{(11)(27)}{(2)(175)}\alpha^4 \right] \frac{\alpha^2\phi_c}{N} \\ & - \left[ \frac{1}{1 + \frac{3}{5}\alpha^2 + \frac{(33)(9)}{(2)(175)}\alpha^4} \right] \left[ \frac{2}{5} + \frac{(2)(99)}{175}\alpha^2 \right] \frac{\alpha^2\phi_c}{N} \\ & - \frac{\phi_c}{N} \left( 1 + \frac{\xi}{v} \right) + \ln(1 - \phi_c) + \phi_c + \phi_c^2 \chi + \frac{\Delta\mu_H}{RT} \end{aligned} \quad (5)$$

where the  $L^*$  distribution has been truncated after the  $\alpha^4$  term.

The results of applying these equations are shown in figures 2 and 3, which shows a plot of the chemical potential as a function of the concentration of coal in the swollen sample. The non-zero intercept corresponds to the reciprocal of the degree of swelling. Calculations were performed using parameters for an Illinois #6 coal swollen in pyridine and THF, as listed in reference 12. We employed the data for swelling in pyridine ( $Q=2.5$  or  $\phi_c=0.4$ ) to calculate the number of statistical units in a chain, and it can be seen that we calculate a value of  $N=2$  for the Gaussian approximation and  $N=4$  using the  $L^*$  distribution. The number of "aromatic clusters" per statistical unit is probably of the order of 5-10 (a statistical unit consists of a sufficient number of segments to give behavior equivalent to that of a freely jointed chain), so that the average number of units between cross link points is probably of the order of 20, if the model is correct.

One test of the validity of the model is the degree to which it can now predict other results. Also shown in figure 2 are calculations of the chemical potential of Illinois #6 coal swollen in THF. Because this solvent hydrogen bonds less strongly than pyridine the driving force for chain expansion is less, so we calculate an equilibrium value of  $\phi_c$  of the order of 0.5, or a degree of swelling  $Q=2$ . This is in good agreement with experiment (14).

#### ACKNOWLEDGMENT

We gratefully acknowledge the support of the Office of Basic Energy Sciences, Division of Chemical Sciences, Department of Energy, under Grant no. DE-FG02-86ER13537.

#### REFERENCES

1. Bastide, J., Candau, S., and Leibler, L., *Macromolecules*, 1981, 14, 719.
2. Bastide, J., Picot, C. and Candau, S. J., *Macromol. Sci., Phys.*, 1981, B19, 13.
3. Bastide, J., Duplessix, R., Picot, C. and Candau, S., *Macromolecules*, 1984, 17, 83.
4. Horkay, F. and Zrinyi, M., in "Biological and Synthetic Polymer Networks", Edited by O. Kramer, Elsevier Applied Science, 1988.

5. Geissler, E., Hecht, M., Horkay, F., and Zrinyi, M., in "Springer Proceedings in Physics", Vol. 42, Edited by Baugartner, A. and Picot, C. E., 1989.
6. Neuberger, N. A. and Eichinger, B. E., *Macromolecules*, 1988, 21, 3060.
7. McKenna, G. B., Flynn, K. M. and Chen, Y. H., *Polymer Communications*, 1988, 29, 272.
8. de Gennes, P. G., "Scaling Concepts in Polymer Physics", Cornell University Press, Ithaca, 1979.
9. Painter, P. C. and Shenoy, S. L., *J. Chem. Phys.* (In Press).
10. Painter, P. C., and Graf, J. and Coleman, M. M., *J. Chem. Phys.*, 1990, 92, 6166.
11. Coleman, M. M., Graf, J. and Painter, P. C., "Specific Interactions and the Miscibility of Polymer Blends", Technomics, Lancaster, PA 1991.
12. Painter, P. C., Park, Y., Sobkowiak, M., and Coleman, M. M., *Energy and Fuels*, 1990, 4, 384.
13. Kovac, J., *Macromolecules*, 1978, 11, 362.
14. Larsen, J. W., Green, T., Kovac, J., *J. Org. Chem.*, 1985, 50, 4729.
15. Flory, P. J., *Statistical Mechanics of Chain Molecules*, Hanser Publishers, Reprinted Edition, 1989.

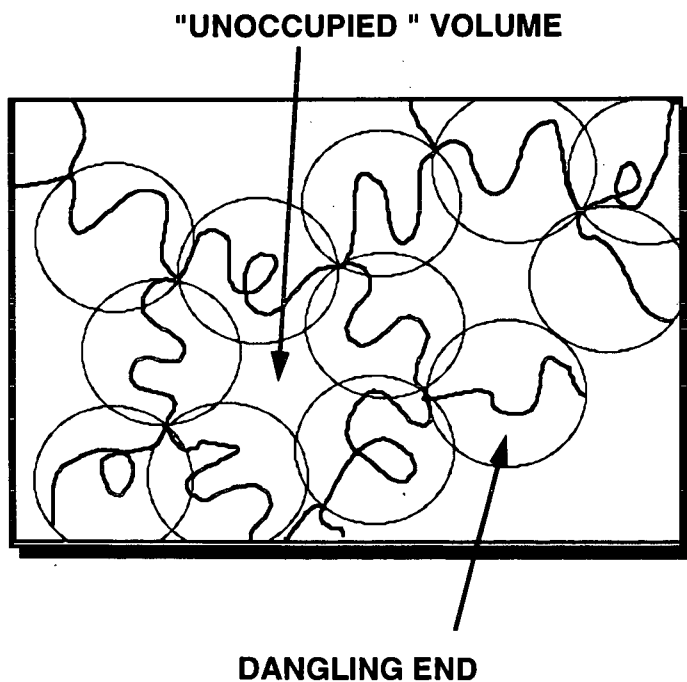
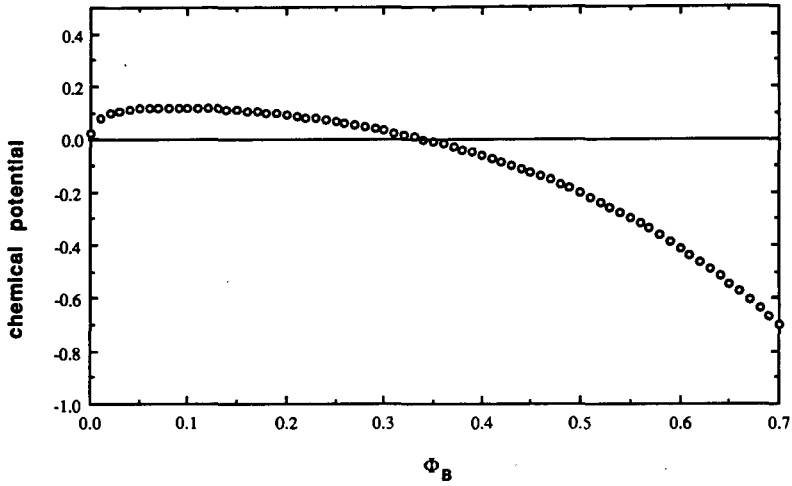


Figure 1. Pictorial representation of the  $C^*$  model of a swollen network

Illinois#6/pyridine n=2 (gaussian)



Illinois#6/thf n=2 (gaussian)

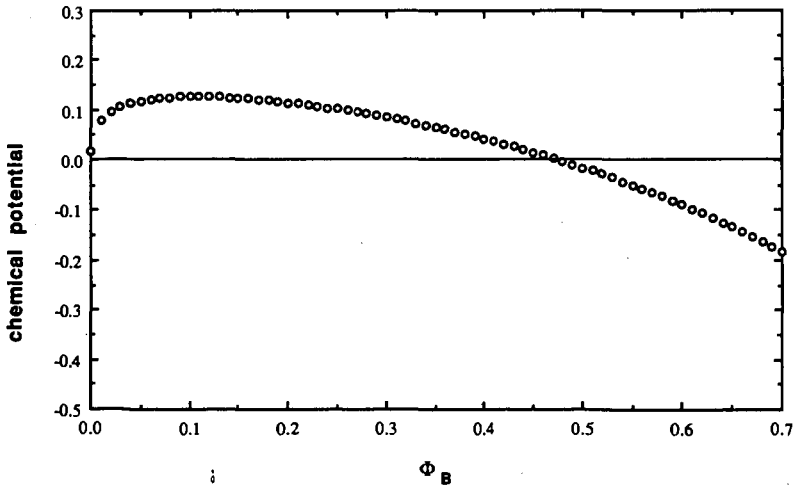
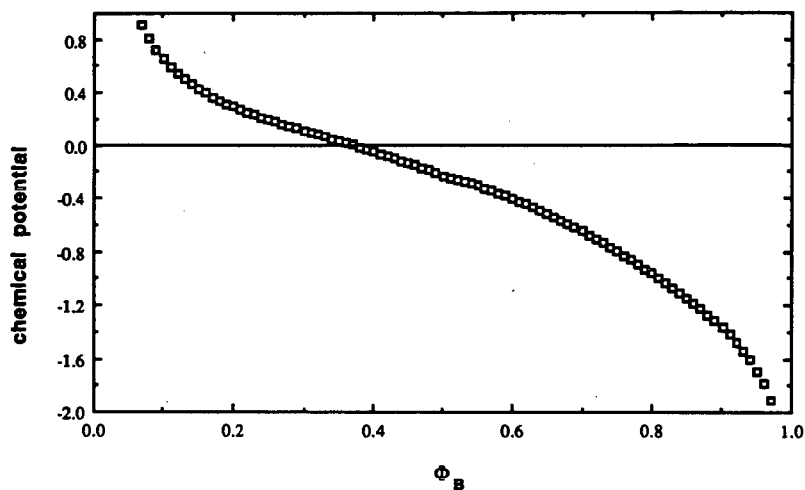


Figure 2. Calculation of the chemical potential as a function of coal segment concentration ( $\Phi_B$ ) in using the Gaussian approximation. Top: Illinois#6 coal swollen in pyridine; Bottom: swollen in THF

Illinois#6/pyridine n=4 (non gaussian)



Illinois#6/thf n=4 (non gaussian)

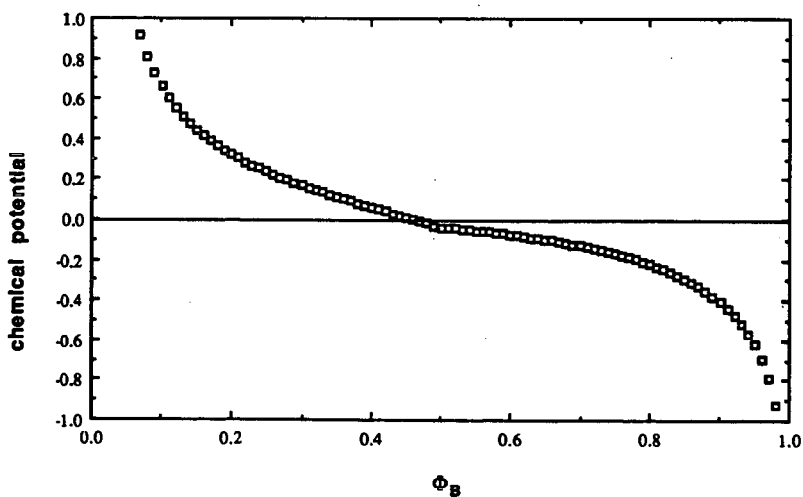


Figure 3. Calculation of the chemical potential as a function of coal segment concentration ( $\phi_B$ ) using the L\* distribution. Top: swollen in pyridine; Bottom: swollen in THF

## NMR IMAGING OF ANOMALOUS SOLVENT TRANSPORT IN MACROMOLECULAR MATERIALS\*

G. D. Cody and R. E. Botto  
Chemistry Division  
Argonne National Laboratory  
9700 S. Cass Avenue  
Argonne, IL 60439

Keywords: NMR, Coal, Polymers, Microscopy

### INTRODUCTION

The phenomenon of solvent transport into polymers has fascinated researchers for decades. Significant insight into the character of solvent transport has been obtained through time resolved direct imaging of concentration gradients during solvent uptake. Early on, optical microscopy revealed that systems in which a change in state accompanies solvent transport exhibit a sharp solvent front that penetrates the sample like a shock wave;<sup>1</sup> such behavior has been referred to as case II transport to distinguish it from Fickian transport. Subsequent analysis of concentration profiles accompanying solvent transport has been accomplished using X-ray absorption<sup>2</sup> and Rutherford backscattering.<sup>3,4</sup> Recently, NMR imaging<sup>5,6,7</sup> has verified the behavioral characteristics of this transport mechanism.

Case II transport behavior has been observed in a wide variety of macromolecule/solvent systems, including complex systems such as bituminous coals swollen in pyridine.<sup>8</sup> The only requirement necessary for case II behavior is that the sample exist in a glassy state when dry, but cross a phase boundary to a rubbery state during the solvent uptake event. Two characteristics which typify case II behavior are the presence of a sharply defined solvent front and a constant front velocity.

The search for a theoretical basis for this type of non-Fickian behavior has been irresistible for both experimentalists and theorists; to date numerous theories abound. Although there are many unique approaches to this problem, it is universally recognized that the general causes of case II behavior are related to the relative magnitudes of characteristic diffusion times and molecular relaxation times in polymer/solvent systems.<sup>9,10</sup> In the present paper, these generalities are exploited for the purpose of simplifying the quantification of case II transport. An experimental analysis of case II transport of methanol in polyethylmethacrylate and pyridine in coal using both optical and NMR imaging techniques is included as a test case for quantifying the transport behavior.

## RESULTS AND DISCUSSION

For the present purposes 2-D images using conventional techniques<sup>11</sup> are sufficient to address the question at hand, and their acquisition is suitably fast. In order to ensure that the transport process was also two-dimensional, the upper and lower sample surfaces were protected from solvent infiltration by glass coverslip which restricted the flow of solvent to cross only the exposed faces of the sample. Each sample is rectangular with initial dimensions on the order of 2 x 2 x 1 mm. The experimental protocol involved immersing the sample in the solvent for a period of time, removing it from the solvent bath, acquiring an image, and re-immersing it.

Figure 1 presents transient images together with one-dimensional projections for each of the three macromolecular systems. The first (a) illustrates the swelling behavior of isobutyl rubber in toluene. In the case of a rubbery material, the transport behavior is anticipated to be Fickian. Analysis of the dynamic behavior of the isobutyl rubber confirms this: during the swelling interval a steep solvent gradient observed in the frame rapidly evolves into a smooth and shallower gradient indicative of a transport mechanism which is essentially Fickian.

The second (b) illustrates the swelling behavior of PEMA in methanol. Clearly evident is a sharply defined solvent front which separates a swollen region from the glassy core. Swelling is essentially complete when the solvent fronts meet at the object center. In general, this behavior is typical of all polymers which pass through a glass to rubber transition during solvent uptake.<sup>12</sup> The term case II has been used to describe such transport phenomena.<sup>1</sup> Analysis of the transport of pyridine during the swelling of a sample of high volatile bituminous coal (c) clearly reveals a sharp concentration profile during the uptake process which is indicative of case II type transport behavior.

In order to quantify the transient aspects of case II transport, a phenomenological transport model was designed which incorporates the essential characteristics of swelling of materials that exhibit a glass transition accompanying solvent uptake. Solvent induced dilation of a macromolecular network, in either the glassy and or the rubbery states, results from osmotic stresses. Kinetically, the character of transport, hence dilation, is different in the two states. In the glassy state the characteristic relaxation time for diffusion is very long relative to the relaxation time for molecular motion. In the rubbery state, however, diffusion is very rapid relative to molecular relaxation. The point of inversion in the relative magnitudes of the characteristic relaxation times occurs when crossing the phase boundary from the glassy to the rubbery state.

The presence of this osmotic stress is a thermodynamic driving force for rapid expansion at the phase boundary. The net effect of the relaxation at the glass to rubber transition is to convert the problem of solvent transport into a moving boundary value problem; the rate of relaxation in the rubbery region drives the diffusion in the glassy region.

Any useful model constitutes a balance between the need to accurately describe a physical process and the desire to remain simple with a minimum number of parameters. Ideally, these parameters have a direct connection with fundamental molecular scale characteristics of the macromolecule. In the case of solvent transport in a system undergoing a glass transition, we can define the uptake behavior using three parameters: a characteristic cooperative diffusion

coefficient,  $D_c$ , governing dilation of the network; a molecular relaxation rate constant,  $\beta$ , which is given by the relationship  $\beta = K_{os}/\eta_l$ , where  $\eta_l$  is the bulk viscosity and  $K_{os}$  is the osmotic modulus; and a critical solvent concentration,  $C^*$ , above which there is a transformation of the network from a glass to a rubber.

Figure 2 illustrates the time dependent uptake,  $L/L_0$ , vs. the square root of dimensionless time,  $\tau$ , for PEMA and the hv bituminous A coal. Depending on the magnitude of  $\beta$ , the characteristic shape of the uptake curve plotted as normalized dilation vs. the square root of dimensionless time is observed to evolve from an essentially convex shape at high values to sigmoid shaped uptake curve at the lower values. The convex curves are indicative of constant velocity of solvent front with time; this is consistent with case II behavior and clearly distinguishable from Fickian transport behavior. The cooperative diffusion coefficient and absolute magnitude of  $\beta$  calculated for PEMA and the coal using  $C^* = 0.25$  are  $D_c = 9.4 \times 10^{-8}$  cm<sup>2</sup>/s,  $\beta = 4.2 \times 10^6$  s<sup>-1</sup> and  $D_c = 7.4 \times 10^{-8}$  cm<sup>2</sup>/s,  $\beta = 3.5 \times 10^6$  s<sup>-1</sup>, respectively. Quantifying these parameters and searching for the relationship between molecular structure and transport behavior will be the focus of future work.

#### ACKNOWLEDGMENT

This work was performed under the auspices of the Office of Basic Energy Sciences, Division of Chemical Sciences, U.S. Department of Energy, under contract number W-31-109-ENG-38.

#### REFERENCES

1. Alfrey, T.; Gurnee, E.F.; Lloyd, W.O. *J. Polym. Sci.* **1966**, *12*, 249.
2. Richman, D.; Long, F. A. *J. Am. Chem. Soc.* **1960**, *82*(3), 509.
3. Hui, C.-Y.; Wu, K.-C.; Lasky, R.C.; Kramer, E.J. *J. Appl. Physics* **1987**, *61*, 5129.
4. Hui, C.-Y.; Wu, K.-C.; Lasky, R.C.; Kramer, E.J. *J. Appl. Physics* **1987**, *61*, 5137.
5. Mareci, T.H.; Donstrup, S.; Rigamonti, A. *J. Mol. Liquids* **1988**, *38*, 306.
6. Koenig, J.L. *J. Appl. Spectroscopy* **1989**, *43*, 1117.
7. Weisenberger, L.A.; Koenig, J.L. *Macromolecules* **1990**, *23*, 2445.
8. Cody, G.D.; Botto, R.E. *Energy & Fuels* **1993**, in press.
9. Hopfenburg, H.B.; Frisch, H.L. *J. Polym. Sci.* **1969**, *7*, 405.
10. Vrentas, J.S.; Jarzebski, C.M.; Duba, J.L. *AIChE J.* **1975**, *21*, 894.
11. French, D.C.; Dieckman, S.L.; Botto, R.E. *Energy Fuels* **1993**, *7*, 90.
12. Thomas, N.L.; Windle, A.H. *Polymer* **1981**, *22*, 627.

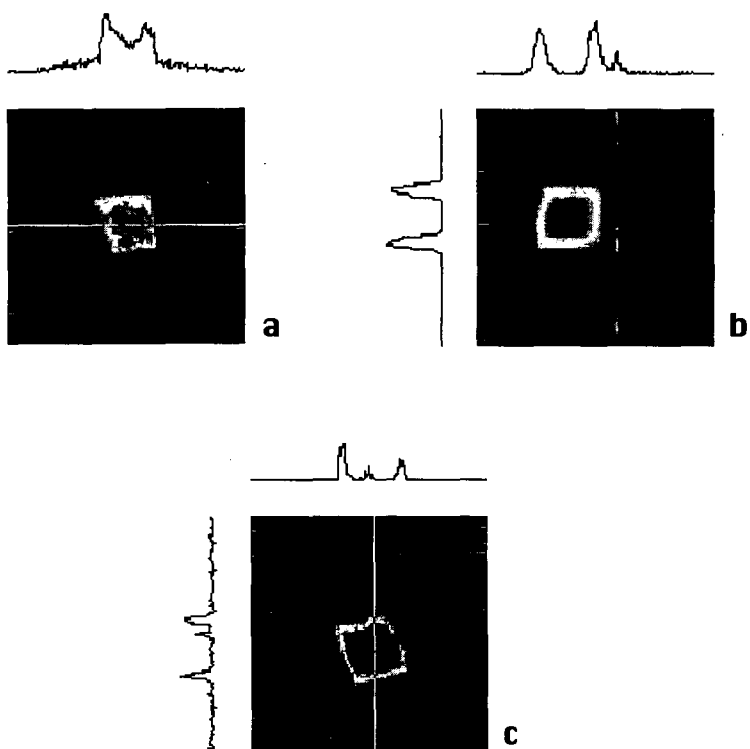


**Figure 1.** 2-D transient proton NMR images and 1-D projections of solvent transport in three macromolecular networks: (a) toluene in isobutyl rubber, (b) methanol in polyethylmethacrylate, and (c) pyridine in hv bituminous A vitrain.

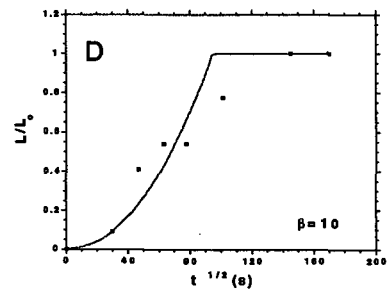
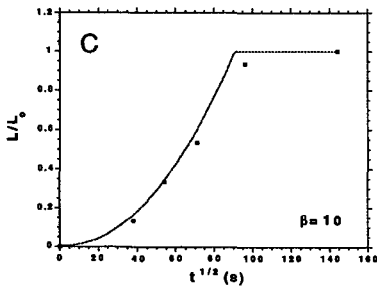
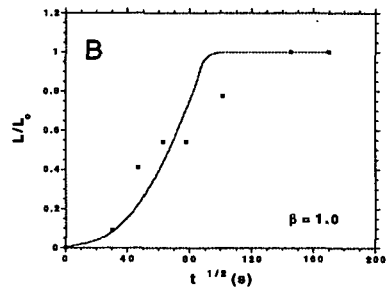
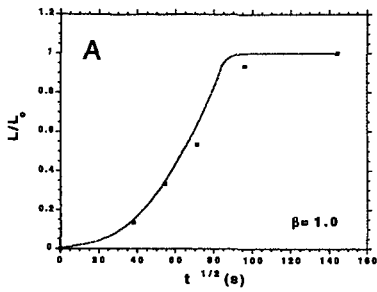


Figure 2. Dilation data for hvA bituminous vitrain swollen in pyridine and polyethylmethacrylate (PEMA) swollen in methanol fit to case II model with  $C^* = 0.25$ : (A) PEMA,  $\beta = 1.0$ ; (B) vitrain,  $\beta = 1.0$ ; (C) PEMA,  $\beta = 10$ ; (D) vitrain,  $\beta = 10$ .

## DUAL MODE SORPTION AND COAL MICROPOROSITY

Thomas K. Green and Trent D. Selby  
Department of Chemistry  
Western Kentucky University  
Bowling Green, KY 42101

Keywords: coal, pyridine, micropores

### INTRODUCTION

Pyridine is one of the most effective and commonly-employed solvents for investigating coal structure. We have recently determined sorption isotherms for several coal-pyridine systems<sup>1</sup>. The most striking characteristic of these isotherms are their high linearity over a very wide pressure range. The curves also have nonzero intercepts. We propose that these isotherms can be modelled by a dual-mode sorption mechanism which has been widely used to interpret the sorption isotherms of glassy polymers.<sup>2-6</sup>

In this model, the sorption mechanism is described in terms of one population of ordinarily dissolved sorbate which resides in the coal matrix and is described by Henry's law (i.e. sorption is linear with pressure) while the second population of sorbate is considered to occupy unrelaxed free volume (micropores) within the coal matrix and is described by a Langmuir isotherm. We propose that the linear portion of the pyridine isotherms presented in this paper represent dissolution of pyridine and that the intercepts are a measure of the coal's microporosity available to pyridine. We present results on the Argonne premium Illinois No. 6 coal, including the whole coal, pyridine extract, extraction residue, and some O-alkylated coals, to support our hypothesis.

### Porosity of Coals.

The pores in porous solids are generally classified into three regimes<sup>7</sup>; macropores with diameters greater than 500 Å, mesopores with diameters from 20-500 Å, and micropores with diameters less than 20 Å. This classification is not arbitrary and is based on the characteristics adsorption effects as manifested in the sorption isotherm. In the macropore range, the pores are so wide that it is virtually impossible to map out the isotherm in detail because the relative pressures of the adsorbate (adsorbed gas) is so close to unity. In mesopores, capillary condensation takes place, usually at moderate relative pressures (greater than 0.3 relative pressure). In micropores, which are of molecular dimensions, an enhancement of the interaction potential takes place between the sorbent and adsorbate. The upper limit of size at which a pore begins to function as a micropore depends on the diameter of the adsorbate molecule; for slit like pores this limit is about 1.5 but for cylindrical pores it lies at a pore diameter of about 2.5 . As a consequence of this enhanced interaction potential, the micropore will be completely filled at low relative pressures, frequently less than 0.01 relative pressure. This paper is concerned with the micropores of coal and this low pressure region where micropores are being filled.

## EXPERIMENTAL

### Sample Preparation

Argonne Premium coals were obtained in ampoules of five grams of - 100 mesh. The coals were first dried under vacuum at 105°C to constant weight and then analyzed for carbon, hydrogen and nitrogen.

Approximately 4.5 g of the sample was Soxhlet-extracted with dry pyridine under argon for several days until the siphon liquid was clear. The pyridine solution was then filtered through a 0.4 m nylon membrane filter to insure removal of particulates and colloidal material. The filter did not plug. Most of the pyridine was removed by rotovaporization under reduced pressure at 70-80°C. Approximately 200 mL of a methanol/water (80/20 vol) mixture and 2 mL of conc. HCl were added to the flask and the mixture was stirred under nitrogen for two days. This treatment was used to remove residual pyridine. The solid extract was then filtered and dried under vacuum at 105°C for 24 h. The extractability was 27.2% (wt) for Illinois No. 6 coal. The extract were analyzed for carbon, hydrogen and nitrogen.

Most of the pyridine was removed from the extraction residues under vacuum. The residues were then treated with HCl/methanol/water and dried in a similar manner as the extracts.

### O-alkylation Procedure.

The procedure for O-alkylation of the Illinois No. 6 coal was conducted according to Liotta's method.<sup>5</sup>

### Sorption Experiments

Sorption experiments on 50 mg samples of the coals were carried out using a quartz spring balance shown in Figure 1. The balance consists of a quartz spring, a 5 L flask, vacuum inlet system, and MKS pressure transducer (0-1000 torr, 0.5% accuracy). The entire balance, including transducer, is housed in a Precision Scientific circulating (forced air) drying oven. The temperature is controlled by a I<sup>2</sup>R temperature regulator, which activates a light bulb.

The sample is suspended from the quartz spring and, as the sample sorbs solvent, the spring extends until equilibrium is reached. The extension of the spring is measured by an Eberbach cathetometer (travelling telescope). The spring is calibrated at the appropriate temperature using standard weights. The balance thus allows determination of the mass of solvent sorbed by the sample at a given partial pressure and temperature. The purpose of the 5 L flask is to minimize pressure changes caused by sorption of solvent by the sample. Quartz springs of the type used here have a linear-extension versus suspended weight relationship and exhibit no hysteresis within the range of weights for which the spring is designed.

## RESULTS

The whole coals, extracts, and extraction residues were exposed to pyridine at various vapor pressures at 50°C. Several incremental sorption experiments were conducted in that, once equilibrium was attained at a particular pressure, the pressure was raised and the system was again allowed to attain equilibrium. Generally one to two days were required for each coal-pyridine system to reach equilibrium at a given pressure. The O-alkylated systems reached equilibrium much faster, typically in less than one hour for the O-butylated and O-

octylated coals at each pressure.

The equilibrium amounts of pyridine sorbed by the coals are plotted against relative pressure of pyridine in Figures 2. For the Illinois No. 6 whole coal, extraction residue, and extract, the isotherms are linear or nearly linear over the relative pressure range of 0.2 to 0.8. For the whole Illinois No. 6 coal, the linear region was found to extend down to 0.05 relative pressure. Additionally, the slopes for the three materials for each coal are similar but the intercepts are quite different. The dramatic increase in intercept upon pyridine-extraction is particularly striking.

We have also determined the sorption isotherms for the three O-alkylated whole Illinois No. 6 coals. The isotherms, shown in Figure 2, are also linear over the range 0.2 to 0.6 relative pressure. The intercept decreases with the size of added alkyl group.

## DISCUSSION

### Dual-Mode Sorption.

We propose that the isotherms can be modelled in terms of a dual-mode sorption mechanism used to explain the sorptive behavior of glassy polymers. This mechanism, introduced by Meares in 1954<sup>3</sup>, and further developed by Barrer et al.<sup>4</sup>, Michaels et al.<sup>5</sup>, and Vieth<sup>6</sup>, describes the sorption mechanism in terms of one population of ordinarily dissolved sorbate which resides in the polymer matrix and is described by Henry's law (i.e. sorption is linear with pressure) while the second population of sorbate is considered to occupy unrelaxed free volume within the polymer matrix and is described by a Langmuir isotherm. This unrelaxed free volume comes about due to restricted rotations of the polymer chains in the glassy state and represents the fixed microvoid or "holes" throughout the polymer. These microvoids act to immobilize a portion of the penetrant molecules by entrapment or by binding at high energy sites at their molecular peripheries (similar to adsorption).

The equilibrium isotherm of the dual sorption model can be expressed by the following equation:

$$C = C_0 + C_H = k_D p + (C'_H b p) / (1 + b p) \quad (1)$$

where C is solubility;  $k_D$  is Henry's Law dissolution constant; b is the hole affinity constant;  $C'_H$  is the hole saturation constant, and p is the pressure. The first term,  $C_0$ , represents sorption of normally diffusible species while the second term,  $C_H$  represents sorption in microvoids or "holes." When  $b p \ll 1$ , the isotherm reduces to a linear form

$$C = [k_D + C'_H b] p \quad (2)$$

At sufficiently high pressures, the microvoids become saturated and will no longer sorb additional penetrant. When  $b p \gg 1$ , sorption in the microvoids reaches a saturation limit,  $C'_H$  and Equation 1 reduces again to a linear form:

$$C = k_D p + C'_H \quad (3)$$

Thus the dual mode sorption model predicts that a plot of C vs p will consist of a low-pressure linear region and high-pressure linear region connected by a nonlinear region.

**Coal-Pyridine Isotherms.** Equation 3 is an equation of a straight-line with a slope of  $k_d$ , the dissolution constant, and an intercept of  $C'_H$ , the hole saturation constant. For the pyridine sorption isotherms shown in Figure 2, we propose that the slopes ( $k_d$ ) are a measure of the solubility of pyridine into the coal matrix and the intercepts ( $C'_H$ ) correspond to the micropore volume available to pyridine. Support for this interpretation includes:

**Isotherm Slopes.** The amount of pyridine sorbed by the whole coal, pyridine-extract, and extraction residue increases linearly with pressure over a wide pressure range (for the whole coal.  $p/p_0$  of 0.05 to 0.8). This Henry's law behavior suggest that dissolution is the dominant process over this pressure range. Moreover, the slopes of the isotherms are very similar for the Illinois No. 6 coal, extract, and residue. Since these materials are all of the same chemical constitution by elemental analysis and NMR analysis<sup>9</sup>, similar slopes are expected if the linear portion of the isotherms represent dissolution of pyridine into the matrix.

It is possible that mesopores are being filled in this high pressure region due to capillary condensation. However, mesoporous solids often exhibit an upturn in the isotherm in the midpressure region<sup>7</sup> which is absent in our isotherms. In addition, pyridine is known to be a good swelling solvent and we can expect the coal to swell (dissolve into the solid) in this pressure region as well. The process of swelling is expected to significantly alter the pore structure of coal in this high pressure region.<sup>10</sup> The remarkable similarity of the slopes of the isotherms for all materials (whole coal, extract, and residue) is, in our opinion, best explained by a dominant process of dissolution of pyridine into the matrix.

**Isotherm Intercepts.** The steep rise in the low pressure region of the whole Illinois No. 6 coal suggests that it is micropores that are being filled, with a corresponding enhancement of the interaction potential and therefore of the enthalpy of adsorption. This enhanced interaction potential will occur at about 1.5 to 2.5 the diameter of the pyridine molecule, depending on whether the pore is slit-like or cylindrical, respectively. The maximum diameter of the pyridine molecule is about 6.8 Å. This suggests a maximum diameter of 17 Å for the diameter of the pores being filled.

The intercept of the isotherm of the Illinois No. 6 whole coal, when converted to a volume of pyridine per g of dmmf coal, agrees well with the micropore volume ( $< 12$  Å) determined for an Illinois #6 coal (PSOC-26) by Walker and coworkers using nitrogen adsorption and mercury and helium displacement.<sup>11</sup> Our value is 0.055 mL/g compared to their value of 0.066 mL/g coal. The agreement is quite good considering that different probes are being used in each case.

**Effect of Pyridine Extraction.** The extraction residues have an intercept two to three times that of the whole coals. According to our interpretation, this is due to a dramatic increase in micropore volume upon pyridine extraction. Solvent extraction has been demonstrated to increase the micropore volume and surface areas for Wyodak subbituminous coal,<sup>12</sup> consistent with these results. The interpretation is that solvent extraction creates new micropores in the coal, thus leading to an increased intercept for the extraction residue.

**Effect of O-methylation.** Pyridine is a polar molecule capable of hydrogen bonding with the hydroxyl groups in the coal. Interaction at these hydrogen bonding sites is expected to be strong in comparison to other interaction sites in the coal and, consequently, pyridine adsorbed at low pressures may preferentially interact at these sites. Thus, one might reasonably expect that the intercepts observed are related to a hydrogen bonding effect.

We have tested this hypothesis by conducting experiments on the O-methylated coal. As seen in Figure 6, O-methylation has little or no effect on the intercept value. Pyridine cannot hydrogen bond to the O-methylated materials. If hydrogen bonding were the cause of the intercepts, the intercepts should be substantially diminished upon hydrogen bonding. That does not suggest another cause for their existence. We argue that the intercepts are related to the microporosity of the coal.

Additionally, the slope of the straight portion of the O-methylated coal is considerably less than that of the whole coal. If the slope is a measure of the solubility of pyridine in coal, then the effect of O-methylation is to reduce the pyridine solubility. This seems logical, given that the O-methylated coal cannot hydrogen bond to pyridine.

**Effect of O-alkylation.** O-alkylation of the whole Illinois No. 6 coal with bulky, alkyl groups results in a reduction of the intercept, consistent with a reduction in micropore volume as the large alkyl groups fill micropores. The intercepts for the series of O-alkylated coals correlate remarkably well with the microporosities measured by Liotta using mercury porosimetry and helium penetration.<sup>8</sup>

Finally, we argue that the micropore volume determined by this technique should be representative of the **unswollen** coal since the micropores are being filled or nearly filled at very low pressures (less than  $p/p_0$  of 0.05 for the whole coal) and swelling by pyridine at these pressures should be minimal. In addition, the micropore volume determined by this method is obtained by **extrapolation** to zero dissolution (or swelling).

#### CONCLUSIONS

Pyridine sorption isotherms for Illinois No. 6 coal give straight-line curves with nonzero intercepts. We have interpreted these lines in terms of a dual-mode model for sorption of gases by glassy polymers. We believe the several lines of evidence discussed above support our interpretation that the intercept values represent micropore volume available to pyridine. Thus, determination of pyridine sorption isotherms may be an effective technique for tracking micropore volume coals and modified coals. Further work is planned to further explore the dual-mode sorption model presented here, with specific attention paid to the low pressure isotherms of these materials.

**Acknowledgement.** The support of the Department of Energy, Grant No. DF-FG22-88PC88924 is gratefully acknowledged.

#### REFERENCES

1. Green, T. K. "Thermodynamics of the Solvent Swelling of Coal," Final Technical Report, DOE/PC/88924, U.S. Department of Energy, Pittsburgh Energy Technology Center, 1991.
2. For a review of this model see Vieth, W. R. Diffusion in and Through Polymers, Hanser Publishers, Munich, 1991, Chapters 2 and 7.
3. Meares, P. J. Am. Chem. Soc. 1954, **76**, 3415.
4. Barres, R. M.; Barrie, J. A.; Slater, J. J. Polym. Sci. 1958, **27**, 177.
5. Michaels, A. S.; Vieth, W. U.; Barrie, J. A. J. Appl. Phys. 1963, **34**, 1-12.
6. Vieth, W. R.; Howell, J. M.; Hsieh, J. H. J. Mem. Sci. 1976, **1**, 177.
7. Gregg, S. J.; Sing, K. S. W. Adsorption, Surface Area and Porosity, Academic Press, London, 1982.
8. Liotta, R.; Rose, K.; Hippo, E. J. J. Org. Chem. 1981, **46**, 277.
9. Davis, M. F.; Quinting, G. R.; Bronnimann, C. E.; Maciel, G.E. Fuel 1987, **68**, 763-770.
10. Winans, R. E.; Thiyagarajan, P. Energy Fuels 1988, **2**, 356-358.
11. Gan, H.; Nandi, S. P.; Walker, P. L. Fuel 1972, **51**, 272.
12. Harris, E. C.; Petersen, E. E. Fuel 1979, **58**, 599-602.

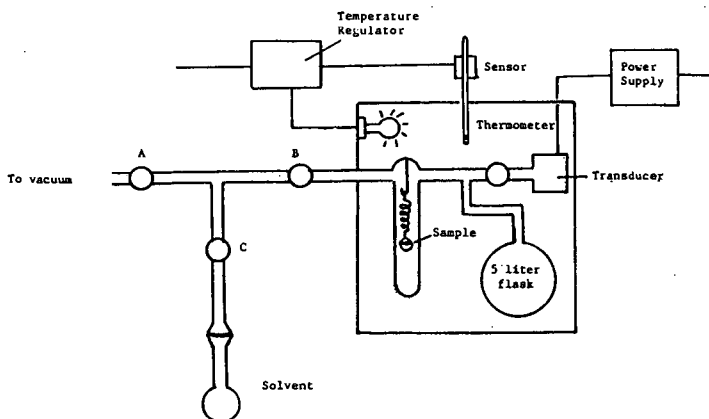


Figure 1. Sorption Apparatus

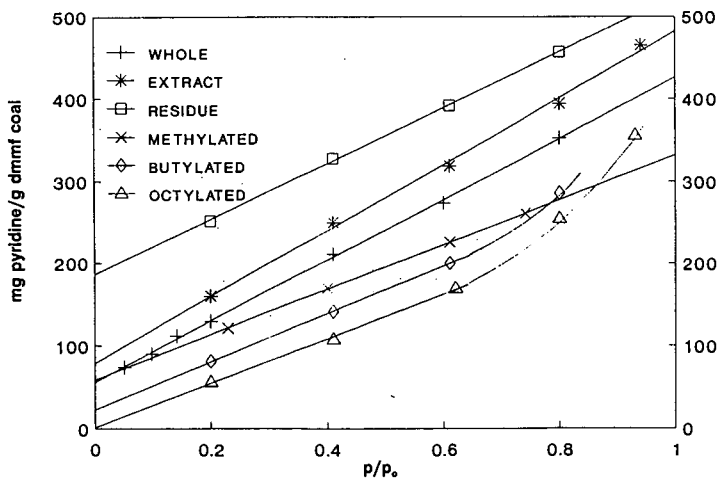


Figure 2. Sorption Isotherms for Illinois No. 6 Coals at 50°C.

## THE EFFECT OF VACUUM DRYING ON MOLECULAR ACCESSIBILITY IN WEATHERED APCS COAL SAMPLES: STRUCTURAL AND CHEMICAL CHANGES

Wojciech Sady, David Tucker, Lowell Kispert and Dennis R. Spears  
Box 870336, Department of Chemistry  
The University of Alabama,  
Tuscaloosa, AL 35487-0336

Keywords: coal structure, vacuum drying, EPR, nitroxyl spin probes

### INTRODUCTION

During weathering, coals are subject to both a loss of water and oxidation, both of which have been shown to have a strong effect on coal conversion.<sup>1,2</sup> Lignites and subbituminous coals can contain over 30% water by weight, so drying is considered to be economically important in the conversion of low ranked coals. The transportation cost alone can be significant. However exposure to air during the weathering process is an important consideration in all coal ranks. Changes in the physical and chemical structure of fresh Argonne Premium Coal Samples (APCS) during weathering have been previously followed using an EPR spin probe technique.<sup>3</sup> This was possible by swelling the coal in a solvent solution of a stable free radical, known as a spin probe, containing a substituent capable of probing the chemical changes in coal. The substituents used in this study contained functional groups capable of being a hydrogen bond donor (-COOH) or a hydrogen bond acceptor (-NH<sub>2</sub>). Removal of the solvent and washing away unreacted spin probes by a non-swelling solvent enabled the weathering process to be monitored by Electron Paramagnetic Resonance (EPR) Spectroscopy. It is the goal of this paper to investigate the changes in APCS coal upon vacuum drying, and to use these results to understand the details of weathering coal in air.

### EXPERIMENTAL

Vials containing the APCS coals were opened in a moisture free, pure argon environment. The characteristics of the coal samples are given elsewhere.<sup>4,5</sup> The coals were vacuum dried in a vacuum desiccator for 18 hours. Weight losses for each coal are given in Table 1. After being weighed, the coals were split into several aliquots. Four of these aliquots for each coal were exposed to air with protection from dust or other contamination insured. The remaining aliquot of each coal was then swelled in a spin probe solution. The samples undergoing weathering were agitated each day to insure thorough exposure to the air. Samples were taken at 8, 14 and 35 days of weathering and swelled in a spin probe solution. The swelling solvent was removed and the spin probe retention was measured by EPR.

The three spin probes used in this study are shown in Figure 1. Spin probes 3-carboxy-2,2,5,5-tetramethylpiperidine-1-oxyl (VI), TEMPAMINE (VII) and TEMPO (VIII), were chosen so that changes in both physical structure and proton donor/acceptor characteristics could be observed. All three have similar molecular volumes, but different chemical reactivities with the coal structure. A detailed description of the experimental method for the intercalation of spin probes using swelling solvents has been previously published.<sup>4,5</sup>

## RESULTS

### Vacuum Drying

Vacuum drying fresh coals caused a weight loss that was consistent with the reported<sup>6</sup> moisture content of each APCS coal. The dried coal increased upon weathering. A typical example is given in Figure 2 for Beulah-Zap lignite where the data of weight loss from the previous study of coal after weathering<sup>3</sup> is plotted with the vacuum dried coal weight change. Both plots converge to a point which represents about 76% of the original water contained in the coal. It would appear that an equilibrium point is reached after approximately 25 days of weathering. For Fresh Beulah-Zap, the weight loss upon weathering was found to have the following dependence on time:

$$\text{Total weight lost} = 26.36x / (2.077 + x), \text{ where } x = \text{days of weathering.}$$

For vacuum dried Beulah-Zap, the weight increase with weathering is :

$$\text{Total weight lost} = 8.838e^{-0.1238x} + 24.10$$

It is clear that during weathering coal reaches a equilibrium where its moisture content is relatively constant.

### Weathering

The spin probe retention for vacuum dried coals, fresh coals and fresh coals weathered in air for one week swelled in a spin probe VI solution of toluene is shown in Figure 3A. All coals except Beulah-Zap show an increase in spin probe retention over fresh coals upon vacuum drying. Illinois #6 at point (g) exhibits the largest increase in retention upon vacuum drying or weathering (over  $2 \times 10^{18}$  spins per gram of coal). Beulah-Zap coal, on the other hand displays a decrease in retention of spin probe VI which is nearly as intense as the increase shown for Illinois #6 coal. It can also be seen that the spin probe retention data for vacuum dried coals and fresh coals weathered for one week are very similar.

Upon vacuum drying or weathering Beulah-Zap, a large decrease in accessibility occurs for spin probe VII in toluene (a), as shown in Figure 3B. Wyodak-Anderson coal likewise exhibits a decrease in retention of spin probe VII upon vacuum drying (f), but weathered Wyodak coal actually displays a slight increase in retention (d). Similar to the results shown in Figure 3A for spin probe VI in toluene, Illinois #6 shows a large increase in retention upon vacuum drying (c). However, fresh weathered Illinois #6 coal does not show any difference in retention over fresh coal (e). The other coals over 81% carbon (dmmf), Blind Canyon, Pittsburgh #8, Lewis Stockton, Upper Freeport and Pocahontas #3, show increased retention upon vacuum drying or weathering and negligible differences in retention for vacuum dried and fresh weathered coal.

Little difference is detected for spin probe VIII retention in toluene for most APCS coals as shown in Figure 3C. Initial vacuum drying has a small effect except for Beulah-Zap which shows a significant decrease in accessibility of spin probe VIII. Blind Canyon coal also exhibits a higher retention for fresh weathered coal over fresh coal to a greater extent than vacuum dried coal (points a and f).

Upon vacuum drying Wyodak-Anderson, a decrease in retention occurs for spin probe VI in pyridine as shown in Figure 4A (a), and a significant increase in retention is observed for Beulah-Zap at point (b). All of the other coals show very little change in retention characteristics upon vacuum drying or weathering.

As shown in Figure 4B at point (a), Illinois #6, Blind Canyon, Pittsburgh #8, Lewis Stockton and Upper Freeport all exhibit unusually high retention of spin probe VII in pyridine upon vacuum drying. Beulah-Zap likewise shows improved retention upon vacuum drying as indicated at point (e), and, in fact, Wyodak-Anderson is the only coal for which vacuum drying produces a significant decrease in spin probe retention.

As seen in Figure 4C for coals swelled in pyridine with spin probe VIII vacuum drying causes an increase in retention for Beulah-Zap and the medium ranked coals.

## DISCUSSION

The results shown in Figure 2 suggest that part of the water in coal is tightly bound since vacuum dried coals absorb water when exposed to air. The data indicates that for Beulah-Zap coal, approximately 76% of the moisture can be easily removed by drying in air and that the remaining 24% requires more intensive methods. This is consistent with other drying studies of lignites and subbituminous coals.<sup>7-9</sup> Recently, Miknis et al. found that after 75% of the water had been removed from Eagle Butte, Wyoming subbituminous coal, greater amounts of energy were required to achieve additional water removal.<sup>7</sup> Likewise, Vorres determined that there were at least two different types of water present in low ranked coal and that a transition to a much slower drying mechanism occurs when 60% - 85% of the water has been removed.<sup>8</sup> This is supported by earlier work with DSC and FTIR results.<sup>9</sup>

In Figures 3A, B and C, a sharp decrease in spin probe retention is observed upon vacuum drying for Beulah-Zap. Since spin probe VIII has no functional group, the decrease in retention upon vacuum drying must be due to either an opening of the structure to such an extent that the spin probe is removed during the cyclohexane wash, or that a structural collapse has occurred upon drying<sup>10</sup> which will not allow any access of even small spin probes to the structure. If the structure were opened extensively, spin probes VI and VII, which exhibit hydrogen bonding, would still show significant retention. This, however, is not observed. Spin probes VI and VII likewise show a decrease of retention in Beulah-Zap upon vacuum drying, verifying that a structural collapse does indeed occur in Beulah-Zap, thus making it inaccessible in toluene.

Illinois #6 swelled in toluene exhibits a significant increase in the retention of spin probes VI and VII upon vacuum drying; for spin probe VI, as much as  $2000 \times 10^{15}$  spins per gram increase. This is shown in Figures 3A and 3B. It may be possible to explain this by assuming that the removal of water increases the number of available polar sites since Illinois #6 contains significant amounts of water, allowing for improved retention of the spin probes. However, Illinois #6 apparently contains enough cross-linking to avoid the structural collapse witnessed in Beulah-Zap.

In pyridine, significantly increased retention of spin probes VI and VII is observed upon vacuum drying in Beulah-Zap, in Figures 4A and 4B. The removal of water from the structure of Beulah-Zap should cause an increase in the number of sites available to these spin probes. While these sites are not accessible in toluene, because of that solvent's inability to reopen the collapsed structure, they are more readily available for interaction when pyridine is used as a swelling solvent because of its ability to disrupt polar interactions in the coal structure, and open up the structure to the spin probes. Looking at spin probe VIII retention in Figure 4C, it can be seen that Beulah-Zap undergoes a structural change upon vacuum drying which is detectable in pyridine, even though pyridine disrupts most hydrogen bonds and other polar interactions.

In Figure 4B, it can be seen that the medium and high ranked coals (Illinois #6, Blind Canyon, Pittsburgh #8, Lewis Stockton and Upper Freeport) swelled in pyridine, all exhibit unusually high retention of spin probe VII upon vacuum drying. This is not observed for spin probe VI shown in Figure 4A. This suggests that active sites are made available upon the removal of water, even in

higher ranked coals, and that the sites must be more acidic (hydrogen bond donating) in nature since selective retention was observed for spin probe VII over VI.

In Figure 3B it is shown that for Illinois #6 swelled in toluene with spin probe VII, a much higher retention for vacuum dried coal than fresh weathered coal is observed. This would suggest that during the weathering process, the coal under goes some changes in chemical structure due to oxidation which is not sensitive to the inclusion of spin probe VI, but causes a decrease in the intercalation of spin probe VII. This indicates a reduction of accessible acid (hydrogen bond donor) sites upon oxidation.

## CONCLUSION

It is shown that the removal of water and volatile components from coal during the weathering process is primarily responsible for the changes which occur in swelling character. It is also verified that the collapse of lower ranked coals during weathering is due to the removal of water. Medium ranked coals appear to have enough crosslinking to resist structural collapse upon water removal, but not enough crosslinking to prevent an opening of the structure upon swelling in mild solvents. Changes in the retention of polar spin probes in Illinois #6 coal swelled in toluene indicate that vacuum drying increases the total number of active sites available for polar interactions, but that oxidation during weathering reduces the number of available hydrogen bond donor sites. It is also shown that the removal of water can increase the retention of polar spin probes in high ranked coals swelled in pyridine.

## ACKNOWLEDGMENT

This work was supported by the U.S. Department of Energy, University Coal Research Program under grant no. DE-FG22-90PC90284.

## REFERENCES

1. Saini, A.K.; Song, C.; Schobert, H.H. *Prepr. Pap. Am. Chem. Soc., Div. Fuel Chem.* **1993**, *38*, 593-600.
2. Saini, A.K.; Song, C.; Schobert, H.H. *Prepr. Pap. Am. Chem. Soc., Div. Fuel Chem.* **1993**, *38*, 601-608.
3. Sady, W.; Kispert, L.D.; Spears, D.R. *Am. Chem. Soc. Fuel Chem. Prepr.* **1992**, *37*, 1151.
4. Goslar, J.; Kispert, L.D. *Energy and Fuels* **1989**, *3*, 589-594.
5. Spears, R.; Kispert, L.D.; Piekara-Sady, L. *Fuel* **1992**, *71*, 1003.
6. Vorres, K. S. *Energy & Fuels* **1990**, *4*, 420-426.
7. Miknis, F.P.; Netzel, D.A.; Turner, T.F. *Prepr. Pap. Am. Chem. Soc., Div. Fuel Chem.* **1993**, *38*, 609-617.
8. Vorres, K.S. *Prepr. Pap. Am. Chem. Soc., Div. Fuel Chem.* **1993**, *38*, 587-592.
9. Vorres, K.S.; Molenda, D.; Dang, Y.; Malhotra, V.M. *Prepr. Pap. Am. Chem. Soc., Div. Fuel Chem.* **1991**, *36*, 108-120.
10. Yost, R. S.; Creasy, D. E. *Fuel*, **1990**, *69*, 648.

Table 1. Weight loss ( $\pm 0.4\%$ ) of APCS coals after vacuum drying.

Coal	Carbon Content	Moisture Content	% Weight Loss
Beulah-Zap	74.05%	32.24%	32.6%
Wyodak-Anderson	76.04%	28.09%	28.0%
Illinois #6	80.73%	7.97%	----
Blind Canyon	81.32%	4.63%	4.7%
Pittsburgh #8	84.95%	1.65%	1.7%
Lewiston-Stockton	85.47%	2.43%	2.2%
Upper Freeport	88.08%	1.13%	1.0%
Pocahontas	91.81%	0.65%	0.8%

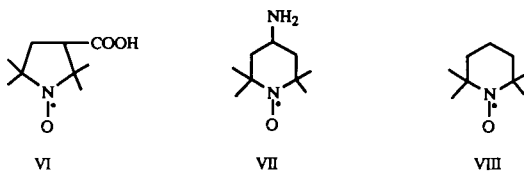


Figure 1. Spin probes VI, VII, and VIII.

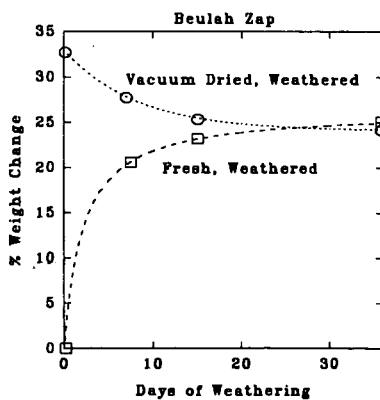


Figure 2. Percent weight change (loss) for (○) vacuum dried and (□) fresh Beulah zap coal weathered in air for 0 to 35 days.

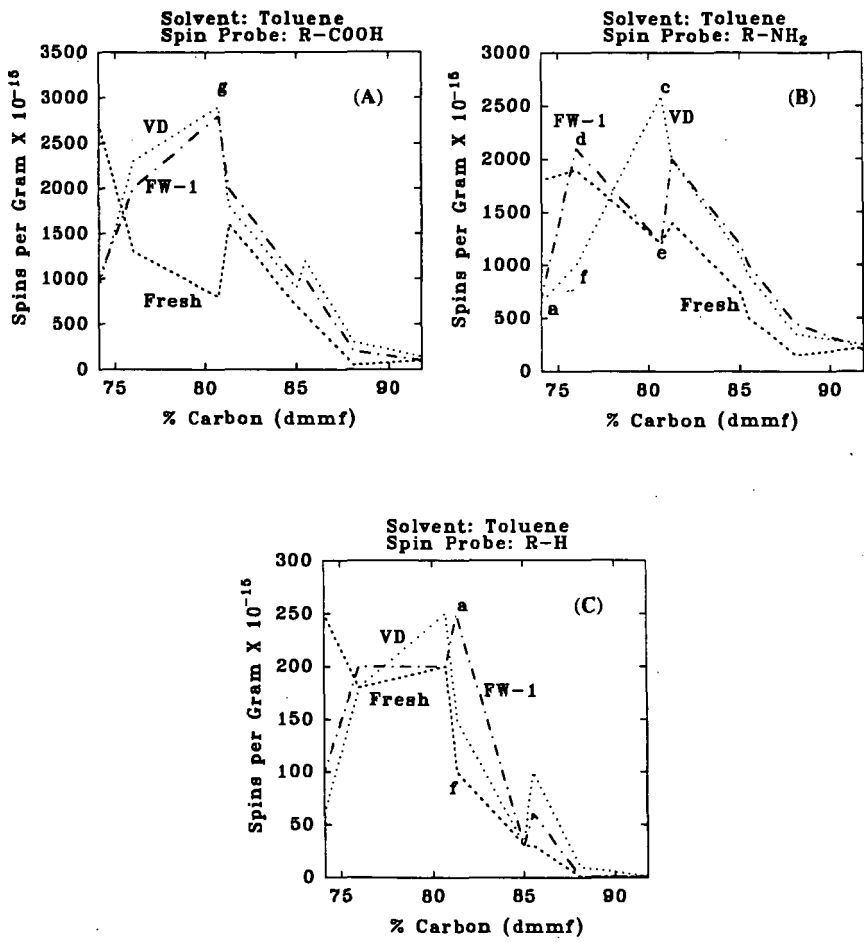


Figure 3. Nitroxide radical concentration in EPR spins per gram of coal vs. percent carbon (dmmf) with toluene as the swelling solvent. For ... vacuum dried coals (VD), --- fresh coals (fresh) and - - - fresh coal weathered for one week (FW-1), (A) using spin probe VI, (B) using spin probe VII and (C) using spin probe VIII.

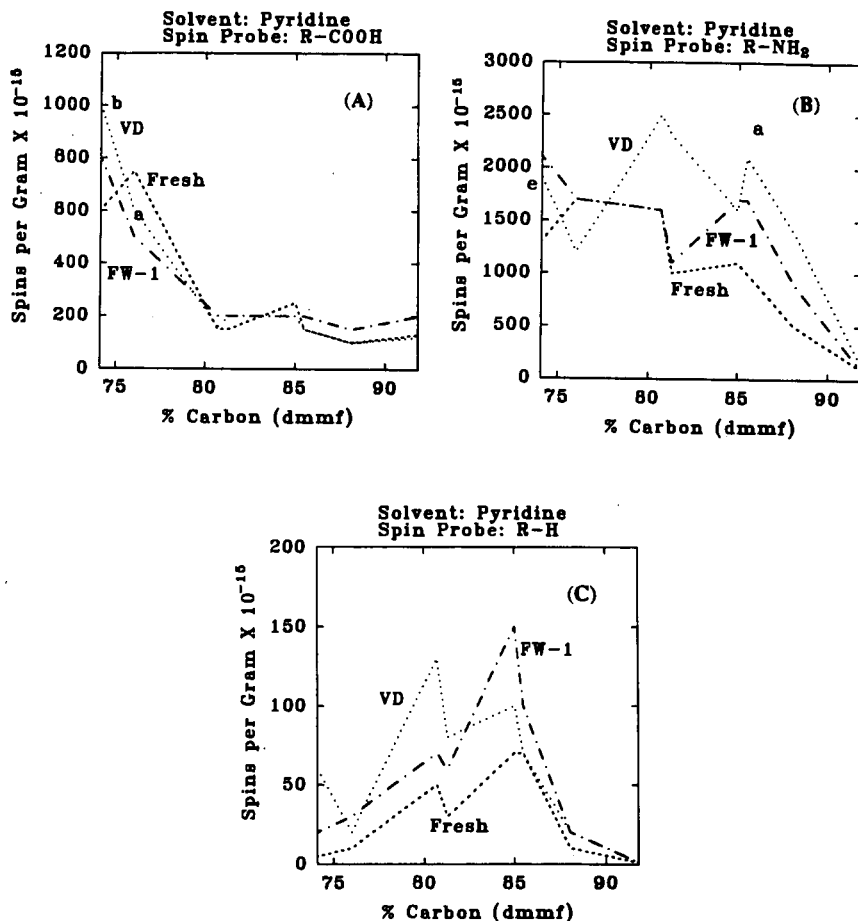


Figure 4. Nitroxide radical concentration in EPR spins per gram of vs. percent carbon (dmmf) with pyridine as the swelling solvent for ... vacuum dried coals (VD), --- fresh coals (fresh and --- fresh coals weathered for one week (FW-1), (A) using spin probe VI, (B) using spin probe VII and (C) using spin probe VIII.

## THE EFFECT OF O<sub>2</sub> OXIDATION VERSUS WEATHERING IN AIR ON THE STRUCTURE OF THE APCS COAL SAMPLES DETERMINED BY THE EPR SPIN PROBE METHOD

David Tucker, Lowell Kispert and Wojciech Sady  
Box 870336, Department of Chemistry  
The University of Alabama,  
Tuscaloosa, AL 35487-0336

Keywords: coal weathering, EPR, nitroxyl spin probe, vacuum drying

### ABSTRACT

Eight vacuum dried Argonne Premium Coal Samples (APCS) were oxidized in a pure oxygen enclosed, moisture free environment, and the effects of oxidation alone on coal structure were studied by the intercalation of EPR spin probes [3-carboxy-2,2,5,5-tetramethylpiperidine-1-oxyl (VI), TEMPAMINE (VII) and TEMPO(VIII)]. These studies clearly differentiated between the effect of oxidation and the effect of moisture removal or addition on the physical and chemical structure of coals. The data shows a factor of 5 increase in spin probe retention for some coals oxidized in O<sub>2</sub> versus air, suggesting a large increase in oxidized material.

### INTRODUCTION

Exposure to air during the weathering process has been previously shown to greatly alter the molecular accessibility of EPR spin probes in coal.<sup>1</sup> Weathered coals are subject to a loss of water and oxidation, both of which have been shown to have a strong effect on coal conversion,<sup>2,3</sup> and the physical and chemical structure of coal.<sup>1</sup> The effect of vacuum drying is also discussed elsewhere.<sup>4</sup> This technique has been very useful in studying molecular accessibility in coal samples.<sup>5-7</sup> Use of spin probes has been shown particularly advantageous when the spin probes contain polar substituents. Lignite and subbituminous coal contain carboxyl and hydroxyl groups. Nitrogen functionalities make only minor contributions in coal due to the low nitrogen content in coal. A spin probe with an amino substituent is a strong hydrogen bond acceptor, capable of only weak hydrogen bond donation. A spin probe with a carboxyl group is a strong hydrogen bond donor, but is only capable of acting as an acceptor through the carbonyl group. Thus these spin probes can interact and detect the presence of hydroxyl and carbonyl groups present in the coal matrix. The effect of size incorporation in the coal matrix can be determined by comparing a spin probe without a substituent (substituted only with a proton) to those similar in size containing a substituent. Solvents like pyridine are capable of hydrogen bonding with coal. Pyridine has been shown to break up the hydrogen bonding cross-links in the coal structure.<sup>6</sup> It is possible to displace hydrogen bonded spin probes with pyridine. It has been shown that the hydrogen bond donating ability increases in the series -H << -OH < -COOH < -NH<sub>2</sub>. This feature is used to deduce the effect of oxidation on coal. It is the goal of this paper to use this technique to investigate the contribution of oxidation on the swelling properties of coal during the weathering process.

### EXPERIMENTAL

Vials containing the APCS coals (defined previously<sup>8</sup>) were opened in a moisture free, pure Argon environment. The coals were vacuum dried in a vacuum desiccator for 18 hours. After being weighed, the coals were split into several aliquots. Five of these aliquots for each coal were

placed under a dry, pure oxygen (99.9995%) environment. The remaining aliquot of each coal was then swelled in a spin probe solution. The samples undergoing oxidation were agitated each day to insure thorough exposure. Samples were taken at 4, 8, 15, 36 and 64 days of oxidation and swelled in a spin probe solution of toluene or pyridine. The swelling solvent was removed and the spin probe retention was measured by EPR. The three spin probes used in this study are shown in Figure 1. The previously published numbering system<sup>1,5-7</sup> has been used.

A detailed description of the experimental method for the intercalation of spin probes using swelling solvents has been previously published.<sup>5-7</sup> Briefly, 30 mg of a coal is swelled in toluene or pyridine under argon with 2 mL of 1 mM solutions of spin probes at about 298 K for 18 hours. The solvent is filtered off and the coal is vacuum-dried at room temperature for 2 hours. The coal is then washed in cyclohexane to remove any spin probes on the coal surface. This procedure also removes any spin probes from the macro or mesopores. The cyclohexane is then removed under vacuum. Finally, the coal is placed in a EPR tube and evacuated. The concentration of spin probes retained in the coal is then determined by EPR.

## RESULTS AND DISCUSSION

The data is plotted three dimensionally for ease of analysis since so many samples were collected. The spin probe retention is expressed in terms of concentration in spins per gram versus the oxidation period in days and % carbon (dmmf) for each spin probe/swelling solvent combination. The coals were vacuum dried and put in a moisture free oxygen environment so that only the effects of oxidation on the coals could be studied. Due to the constraints of the limited available space for this paper, only the results for coals swelled in toluene with spin probe VI will be discussed. Spin probe VI was chosen because of its versatility in polar interactions.

Figure 2 represents the effects of oxidation on vacuum dried coals swelled in toluene with spin probe VI. The front edge parallel to the Days of Oxidation axis shows the transition that Beulah-Zap goes through during the oxidation process with respect to the polar spin probe VI. It is shown that Beulah-Zap undergoes by a structural collapse upon vacuum drying. Little change in retention is observed during the first eight days of oxidation. However, after eight days, a continued increase in retention of spin probe is observed until after 64 days a retention of  $7.2 \times 10^{18}$  spins per gram is observed. The structure must open during the oxidation process such that large amounts of spin probe VI are retained, because toluene is known to have little effect on breaking cross-links or other intramolecular interactions.<sup>6</sup>

Wyodak-Anderson, like Beulah-Zap, starts out with very little retention of spin probe VI and is not significantly affected by oxidation until 8 days of exposure to oxygen. At 8 days, the spin probe concentration increases to about  $4 \times 10^{18}$  spins per gram (shown in Figure 2 at point f). However, after the increase at 8 days, there is little change until 64 days of exposure where at point a sudden relative decrease in spin probe retention is observed. This would indicate a structural change where the spin probe was no longer able to access the coal structure, or a change in chemical structure which would limit the polar interactions between the coal structure and the spin probe.

Blind Canyon exhibits a decrease of spin probe retention after 8 days of exposure to oxygen (point d), followed by a steady increase in retention of spin probe VI until at 64 days of exposure to oxygen (point b), it retains nearly  $1 \times 10^{19}$  spins per gram, which is five times the amount retained in Blind Canyon coal weathered for 64 days, indicating a large increase in oxidized material.

The higher ranked coals, (Pittsburgh #8, Lewis Stockton, Upper Freeport and Pocahontas #3) which showed little change upon vacuum drying for coals swelled in toluene for spin probe VI, show significant changes in retention characteristics after just four to eight days of oxidation in oxygen (see area e in figure 2 or the expansion of Figure 2 given in Figure 3). For example, after 8 days of exposure to oxygen, Upper Freeport shows a retention of  $3.7 \times 10^{18}$  spins per gram. Initially, the spin probe retention was  $1.1 \times 10^{17}$  spins per gram while the highest retention observed for Upper Freeport coal weathered in air for 8 days was  $4.5 \times 10^{17}$  spins per gram. Both of these results are around an order of magnitude less than the results obtained for Upper Freeport oxidized in oxygen.

The effect of weathering vacuum dried coals in air and the effect of weathering fresh coals in air are presented in Figures 4 and 5A respectively for measurements of the retention of spin probe VI for 36 days. It is apparent that oxidation has a larger effect on molecular accessibility than vacuum drying during the weathering process (see previous paper).<sup>4</sup> However, the presence of water greatly affects oxidation of coals and alters the retention characteristics of most coals. It is noteworthy to compare the results of the oxidation of vacuum dries APCS coals in  $O_2$  given in Figure 2 for 64 days with a similarly plotted curve (Figure 5B) for spin probe VI for fresh APCS coals weathered in air. By comparing Figures 2 and 5B, it can be seen that oxidation of coals for up to 64 days can result in a large increase in accessibility for polar spin probes into the coal structure, even for higher ranked coal.

## CONCLUSION

Since it has been previously established<sup>1</sup> that Beulah-Zap undergoes a structural collapse, and no water is available to reopen the structure, it can be seen that oxidation can cause changes in the physical structure of low ranked coal. Medium ranked coal, especially Blind Canyon, exhibits a large increase in retention with exposure to oxygen, up to five times greater retention than coal weathered in air for similar periods. This suggests that medium ranked coal increases in oxidized material to a significant extent. Higher ranked coals, which do not exhibit large changes in accessibility upon vacuum drying or weathering, show large increases in retention of polar spin probes upon oxidation in oxygen. A comparison of 3 dimensional plots for vacuum dried coals oxidized in oxygen, vacuum dried coals weathered in air and fresh coals weathered in air shows that oxidation can have a large effect on the accessibility of polar spin probes in coal. By comparing features of these plots, it is possible to distinguish the effect of oxidation in the weathering process from water loss. Not shown or discussed are the results obtained for changing swelling solvents from toluene to pyridine, nor the effects of the change in spin probe functionality and the donor/acceptor properties of the constituents.

## ACKNOWLEDGMENT

This work was supported by the U.S. Department of Energy, University Coal Research Program under grant no. DE-FG22-90PC90284.

## REFERENCES

1. Sady, W.; Kispert, L.D.; Spears, D.R. *Am. Chem. Soc. Fuel Chem. Prepr.* **1992**, *37*, 151.
2. Saini, A.K.; Song, C.; Schobert, H.H. *Prepr. Pap. Am. Chem. Soc., Div. Fuel Chem.* **1993**, *38*, 593-600.



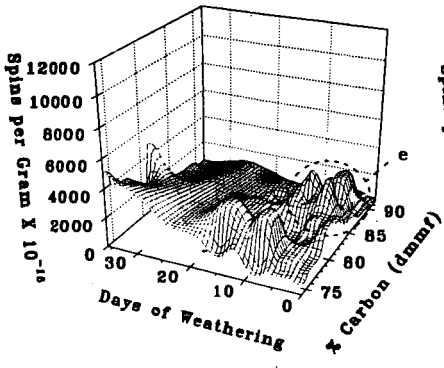


Figure 3 Retention of spin probe VI in vacuum dried coal swelled in toluene expressed as concentration in spins per grams  $\times 10^{-15}$  versus days of exposure to oxygen and % carbon (dmmf). Expansion of Figure 2 for the first 36 days.

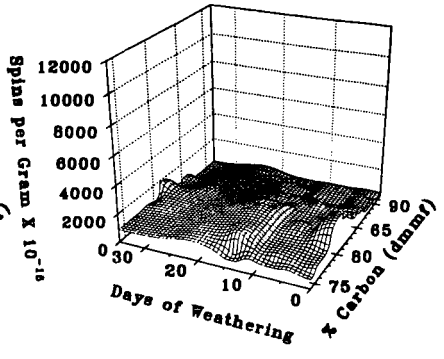


Figure 4 Spin probe VI retention in vacuum dried coal swelled in toluene in spins per gram  $\times 10^{-15}$  vs. days of exposure to air and % carbon (dmmf) for up to 35 days.

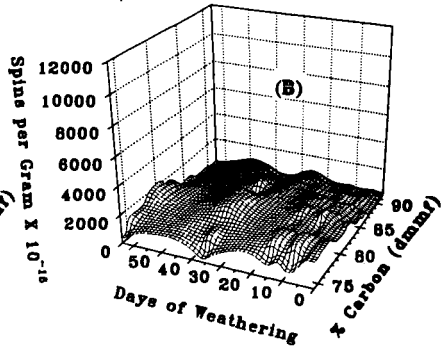
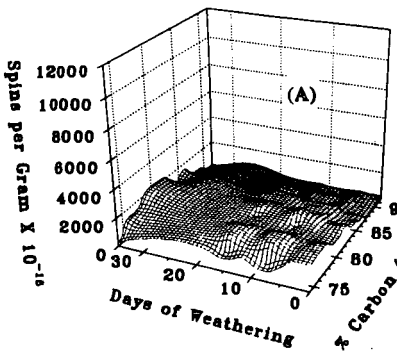


Figure 5. Retention of spin probe VI in weathered, fresh coal swelled in toluene expressed as concentration in spins per gram  $\times 10^{-15}$  versus days of exposure to air and % carbon (dmmf) for up to: (A), 36 days and (B), 64 days.

## AN EPR SPIN PROBE STUDY OF THE EFFECTS OF SHORT TERM OXIDATION AND DEHYDRATION ON THE MOLECULAR ACCESSIBILITY IN ILLINIOS #6 COAL

David Tucker and Lowell Kispert  
Box 870336, Department of Chemistry  
The University of Alabama  
Tuscaloosa, AL 35487-0336

KEYWORD: coal structure, coal dehydration, coal oxidation, EPR spin probes

### ABSTRACT

The effects of short term oxidation and dehydration on the structure and chemistry of the intercalation of potential catalysts into a coal structure during swelling was accomplished using the EPR spin probes 3-carboxy-2,2,5,5-tetramethylpiperidine-1-oxyl (VI), TEMPAMINE (VII) and TEMPO (VIII) as guest molecules. Samples of Illinois #6 APCS coal were exposed to both oxygen and argon for time periods from 30 seconds to 50 minutes after removal from the sealed ampules. The results show that dehydration significantly affects the retention of spin probes with polar functional groups in as little as 30 seconds. It is also observed that structural changes upon exposure of the coal sample to air occur in under 5 minutes. The individual contributions of dehydration and oxidation are discussed.

### INTRODUCTION

Exposure of coal to air before conversion has been a big concern in coal chemistry.<sup>1</sup> It has been suggested that the structure of coal can be altered in as little as two minutes exposure to air.<sup>2</sup> If so, this would make it difficult to carry out accurate structural studies on coal. The previous papers have shown that both dehydration and oxidation<sup>3</sup> change the physical and chemical structure in coal enough so that the molecular accessibility in coal is significantly altered. It is the goal of this paper to determine how quickly and to what extent oxidation or dehydration can affect the structure of coal using the EPR spin probe technique.<sup>3-6</sup> From the previous paper, it was determined that Illinois #6 coal would exhibit the greatest changes in structure upon dehydration and oxidation. Lower ranked coals are more affected by water removal, but do not show as much change during oxidation. A flow of dry oxygen over the coal would result in both loss of water and oxidation. A flow of argon, however, would result in only dehydration since it is inert. By comparing the difference in the effects of both gases on coal, the effects of oxidation alone can be determined. Argon was chosen as the inert gas because of its ability to cover the samples completely with far less difficulty than nitrogen or other inert gases commonly used. Toluene was chosen as a swelling solvent because it does not significantly open the structure of the coal yet allows for diffusion of the spin probes into the available structure. Pyridine was used because it completely opens up the structure and allows for examination of hydrogen bonding sites in coal. Spin probe VIII is a small spherically shaped molecule with no polar substituents. The intercalation of this spin probe simply measures physical changes in the coal structure. Spin probe VI has a carboxyl group and is a hydrogen bond donor with the ability to detect polar interaction in the coal. Spin probe VII has an amino group and is a hydrogen bond acceptor with a much stronger ability to detect polar interactions than spin probe VI. By comparing the retention data for all three spin probes, a more complete picture of the nature of the probe-coal interactions can be obtained.

## EXPERIMENTAL

The vial containing the APCS coal<sup>7</sup> Illinois #6 was opened in a moisture free, pure argon environment and aliquots of coal immediately placed into an apparatus constructed to allow the flow of only pure argon or oxygen over the surface of the fresh coal. A sample of fresh coal was also swelled in each of the spin probe solutions to establish a point of no oxidation or dehydration. It should be noted that the coal was exposed to the argon environment for 10 to 15 seconds before it was placed into the swelling solvent. One aliquot of the coal was exposed to argon and the other to oxygen. A flow of approximately 40 mL per minute of each gas was maintained through the coal sample for 30 seconds, 5 minutes and 50 minutes. The coal was then swelled in a spin probe solution of toluene or pyridine for 18 hours. The swelling solvent was removed and the spin probe retention was measured by EPR. Samples were replicated so that some indication of reproducibility could be obtained.

The three spin probes used in this study are shown in figure 1. Spin probes 3-carboxy-2,2,5,5-tetramethylpiperidine-1-oxyl (VI), TEMPAMINE (VII) and TEMPO (VIII), were chosen so that changes in both physical and chemical structure could be observed. All three have similar molecular volumes, but different chemical reactivities with the coal structure.

A detailed description of the experimental method for the intercalation of spin probes using swelling solvents has been previously published.<sup>4-6</sup>

## RESULTS AND DISCUSSION

The effects of exposure of Illinois #6 swelled in toluene to both argon and oxygen on the retention of spin probe VI are shown in Figure 2(A). Dramatic effects are seen on the retention of spin probe VI after just 30 seconds. After 30 seconds, a decrease of over  $1200 \times 10^{15}$  spins per gram is observed for coal exposed to argon. The decrease in retention is somewhat less pronounced for exposure to oxygen. After 5 minutes of exposure to argon, the retention characteristic of Illinois #6 returned to that found for fresh coal. The increase for oxygen followed the same trend, but to a far less extent. At 5 minutes, the difference between dehydrated (argon only) and oxidized coal is significant. This difference becomes more pronounced after 50 minutes of exposure. In the first 5 minutes, oxidation seems to cause changes which counteract the effects of dehydration. Beyond 30 seconds, oxidation caused a decrease in the retention of spin probe VI, indicated by the increasing retention difference with exposure to oxygen as compared with argon. At 5 minutes or more, dehydrated coals (argon) have a much higher retention of spin probe VI than dehydrated and oxidized coal.

The effects of dehydration and oxidation on the retention of spin probe VII in Illinois #6 coal swelled in toluene are shown in Figure 2(B). A decrease in spin probe retention of  $2500 \times 10^{15}$  spins per gram is observed upon exposure to either argon or oxygen for 30 seconds. This change represents an order of magnitude decrease in spin probe VII retention. This is followed by an increase in retention at 5 minutes of exposure, and then a more gradual decline in molecular accessibility for exposure up to 50 minutes. These results are similar to those obtained for spin probe VI in Figure 2(A) except that after 30 seconds, the coal exposed to oxygen shows improved retention over coal exposed to argon. This difference becomes less significant after 50 minutes of weathering. Again, the shape of each plot is very similar, indicating that the more severe changes are caused by dehydration rather than oxidation.

Structural changes in Illinois #6 coal swelled in toluene can be observed in Figure 2(C) by the retention of spin probe VIII. The plots generated are very similar to those shown in Figure 2(A) for spin probe VI. A decrease in retention is observed in the first 30 seconds, followed by an

increase at five minutes and a gradual decrease in retention up to 50 minutes. The increase in spin probe retention exhibited at 5 minutes of exposure is much greater for coal exposed to argon than oxygen. The initial decrease in spin probe concentration is most likely due to a structural collapse or increased cross-linking, making the structure less accessible since the structure was likewise inaccessible to spin probes VI and VII. It also appears that the changes which occur due to oxidation counteract (to a limited degree) the changes brought about by dehydration in the first 5 minutes. Figure 2(C) shows that some of the effect seen in Figures 2(A) and 2(B) are due to changes in the physical structure since spin probe VIII has no reactive substituents, and shows similarly shaped plots. It is important to note that a retention of nearly  $500 \times 10^{15}$  spins per gram is observed after 30 seconds of exposure to argon. This figure is at least double any of the spin probe VIII concentrations found in Illinois #6 coal fresh, vacuum dried or weathered in air.

When Illinois #6 is exposed to oxygen and argon and then swelled in pyridine in the presence of spin probe VI, retention characteristics exhibit changes illustrated in Figure 3(A) which are similar to those shown for coal swelled in toluene. A decrease in spin probe retention is observed after 30 seconds of exposure to oxygen or argon. Although this decrease is quite small in comparison to those shown for polar spin probes in toluene, it does indicate that the inaccessibility of these spin probes at 30 seconds of exposure is not entirely due to changes in physical structure, since pyridine is capable of disrupting most polar interactions in coal. Again, after 5 minutes of exposure, the retention of spin probe VI is increased to a point which is considerably greater than the initial retention, more so for coal exposed to oxygen than argon. As the time of exposure is extended to 50 minutes, the retention of spin probe VI in dried (exposed to argon) coal increases slightly while the retention in oxidized (exposed to oxygen) coal decreases.

The results of changes in the retention of spin probe VII in Illinois #6 coal upon exposure to oxygen and argon are shown in Figure 3(B). As seen in the previous figures, a decrease in retention is observed for exposure to both oxygen and argon, but more so for oxygen. After 5 minutes in argon, the coal exhibits improved retention, far surpassing the accessibility of the fresh coal. Five minutes of exposure to oxygen does cause an increase in retention from the 30 second exposure, but the increase is still below the retention in the original fresh coal. After an exposure of 50 minutes, the retention of spin probe VII under both circumstances, increases (although to a greater extent in oxidized coal). It would appear that within the first 5 minutes, oxidational changes inhibit the accessibility of spin probe VII into the coal structure.

The retention of spin probe VIII in Illinois #6 coal upon exposure to argon and oxygen for up to 50 minutes is shown in Figure 3(C). Very little change in the structure is observed for 30 seconds of exposure. After 5 minutes of exposure, however, increase retention was observed for both dried and oxidized coal. This is particularly pronounced for oxidized coal. As the exposure time continues beyond five minutes, the retention of spin probe VII in coal exposed to oxygen decreases significantly, while the retention in coal exposed to argon increases. It is clear that oxidation has an effect on the physical structure of the coal which can suppress changes caused by water loss.

A comparison of Figures 2(A) to 2(C) and 3(A) to 3(C) shows that the retention characteristics of spin probe VI closely mirror those of spin probe VIII. This would suggest that changes in the physical structure of coal can influence the retention of spin probe VI as well. Also since oxidation produces an increase in retention of spin probe VII in coal swelled in toluene, but a decrease in the retention of spin probe VI, it would seem that oxidation causes an increase in active sites capable of being hydrogen bond donors.

## CONCLUSION

It is clearly shown that significant structural changes in Illinois #6 can occur in as little as 30 seconds of exposure to a dry gas environment. This should be taken into consideration when the use of an experimental method to determine the structure of coal requires exposure to air for any length of time.

## ACKNOWLEDGMENT

This work was supported by the U.S. Department of Energy, University Coal Research Program under grant no. DE-FG22-90PC90284.

## REFERENCES

1. Yongseung, Y.; Suuberg, E. M. *Prepr. Pap. Am. Chem. Soc., Div. Fuel Chem.* **1992**, *37*, 1184-1192.
2. Graff, R. A.; Brandes, S. D. *Energy & Fuels* **1987**, *1*, 84.
3. Sady, W.; Kispert, L. D.; Spears, D. R. *Am. Chem. Soc. Fuel Chem. Prepr.* **1992**, *37*, 1151.
4. Goslar, J.; Kispert, L. D.; *Energy and Fuels* **1989**, *3*, 589-594.
5. Spears, R.; Kispert, L. D.; Piekara-Sady, L. *Fuel* **1992**, *71*, 1003.
6. Spears, D. R.; Sady, W.; Kispert, L. D. *Fuel* **1993**, *72*, 000.
7. Vorres, K. S. *Energy and Fuels* **1990**, *4*, 420-426.

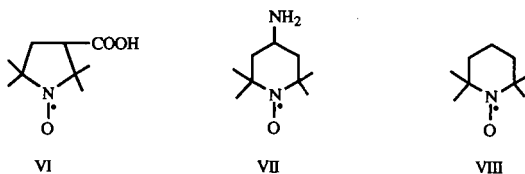


Figure 1. Spin probes VI, VII, and VIII

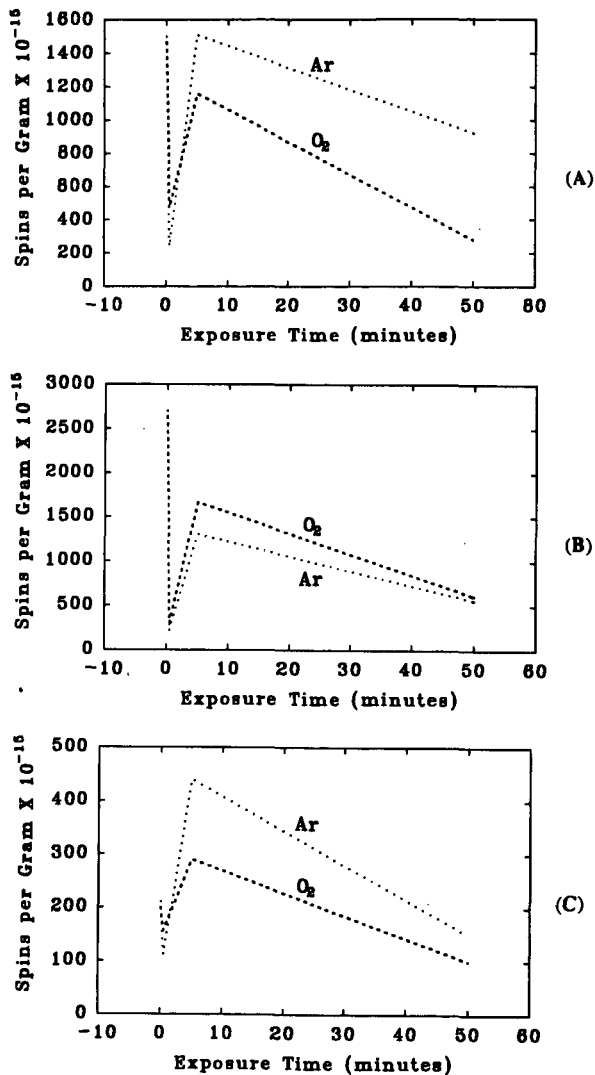


Figure 2. The retention of spin probes (A) VI, (B) VII and (C) VIII in Illinois #6 APCS coal swelled in toluene versus exposure to oxygen or argon in minutes.

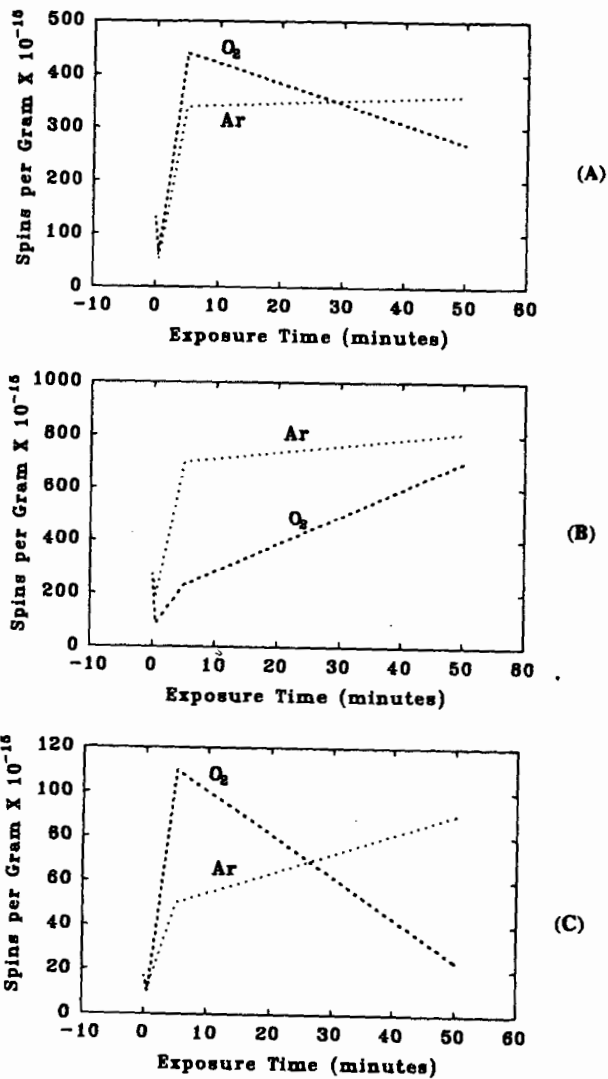


Figure 3. The retention of spin probes (A) VI, (B) VII and (C) VIII in Illinois #6 APCS coal swelled in pyridine versus exposure to oxygen or argon in minutes.